2018

THE EFFECT OF NI ON THE SECONDARY CORROSION PROTECTION OF FE BASED MODEL ALLOYS AT 600 °C

AUTHORS:
DOUGLAS OLLHAGE
CARL LAURELL

SUPERVISION TEAM:
DR. TORBJÖRN JONSSON
JULIEN PHOTHER
JOHAN EKLUND

EXAMINER:
PROFESSOR JAN-ERIK SVENSSON

Abstract

The formation of secondary protective oxides has been investigated for three different alloys with different wt% nickel. The presence of alkali salts causing severe corrosion of stainless steel in biomass- and waste- fired boilers. All the alloys showed a breakdown of the primary protective oxide scale after exposure to K_2CO_3 and KCl for 24 hours at 600°C. The samples were sprayed with 1 mg/cm^2 of saturated alkali salts before being placed in the furnace. An increased amount of nickel resulted in an increased formation of nickel oxide (NiO) and a decreased formation of iron oxide (Fe_2O_3). The increase in formation of nickel oxide showed a connection to lower mass gain for all the samples exposed to alkali salts. The nickel oxide was shown to grow slower than the iron oxide and had better protective properties. The alloy containing 34 wt% nickel was specifically targeted by water containing environment.

Table of content

Intro

The influence of human activities on greenhouse gas emissions is reaching critical levels, with the potential to alter the climate on earth. It is estimated that the ecological footprint of humans has exceeded the earth's capacity by 60% and 2 thirds of the total ecological footprint can be deduced to CO_2 emissions. [1][2] The continued emissions of carbon dioxide is predicted to have devastating effects on the planet as around 50% of current emissions are absorbed by earth's ecosystems. This has prompted a demand for CO_2 neutral energy sources. [3]

The EU has set targets of decreasing CO_2 emissions by 2020 by 20% relative to 1990. Also setting a target for 10% of all transport fuel to come from renewable sources, such as biofuel. [4] To reach these goals focus has been put on using biomass and waste as energy sources. If the industries producing biomass are conducted in a sustainable manner, the net amount of carbon dioxide does not increase in the atmosphere. The energy produced from burning biomass also has to equal out transport of the biomass while still producing electricity at an economically viable rate [5].

To produce electricity, biomass and waste is used as a CO_2 neutral source of energy. The biomass and waste is burned in boilers in the same way as fossil fuels are burned for electricity production. However biomass and waste fired boilers have a significantly lower electric efficiency than fossil fuel fired boilers. The main reason for the low efficiency of biomass- and waste fired boilers is the low steam temperature generated from burning waste and biomass. The steam temperature has to be limited to reduce the corrosion rate. Corrosion of the metal structure inside the boiler leads to degraded mechanical properties and eventually component failure. [6] [7] Burning waste and biomass creates a complex environment inside the boiler, containing different potassium and chlorine compounds. These compounds are prone to break the protective oxide of the metal alloy and cause break away corrosion. The corrosive compounds combined with the high temperature results in high corrosion rates inside in the boiler [8]. To avoid component failure the structure in the boiler has to be replaced, consecutively leading to high maintenance cost and less produced electricity per time unit.[6] It is necessary to limit the corrosion rate while still maintaining a high steam temperature to ensure an economically viable efficiency of the boiler. A more corrosion resistant alloy or an altered composition of the flue gas are potential solutions.

Aim

The aim of this study is to investigate the effect of nickel content in stainless steels on the secondary protection (after breakaway oxidation) at medium high temperatures (600 °C). Several model alloys with varying nickel contents will be exposed in different corrosive environments.

Theory

Oxidation:

Thermodynamics:

Most metals are thermodynamically unstable under conditions where they are exposed to oxygen. Reacting with the oxygen, the metal tends to form corresponding metal oxides as it can be seen in Reaction 1 below:

(1) $(2a/b)Fe\ (s) + O_2\ (g) <-> (2/b)Fe_aO_b\ (s)$

The reaction depends thermodynamically on the change of Gibbs free energy under constant temperature and pressure. To predict if the reaction is possible to spontaneously occur ΔG can be used as an indicator, where the possibility depends on ΔG to be negative [9]. ΔG can be calculated according to the Formula:

$\Delta G = \Delta G^* + RT\ln(a_{MxOy}{}^{2/y})/((a_M{}^{2x/y})*(a_{O2}))$ [10]

Oxidation of a metal occurs when the partial pressure of oxygen is higher than the equilibrium partial pressure of oxygen at a given temperature. The Ellingham diagram can therefore predict under which conditions a metal will reduce or oxidize [10], see Figure 1.

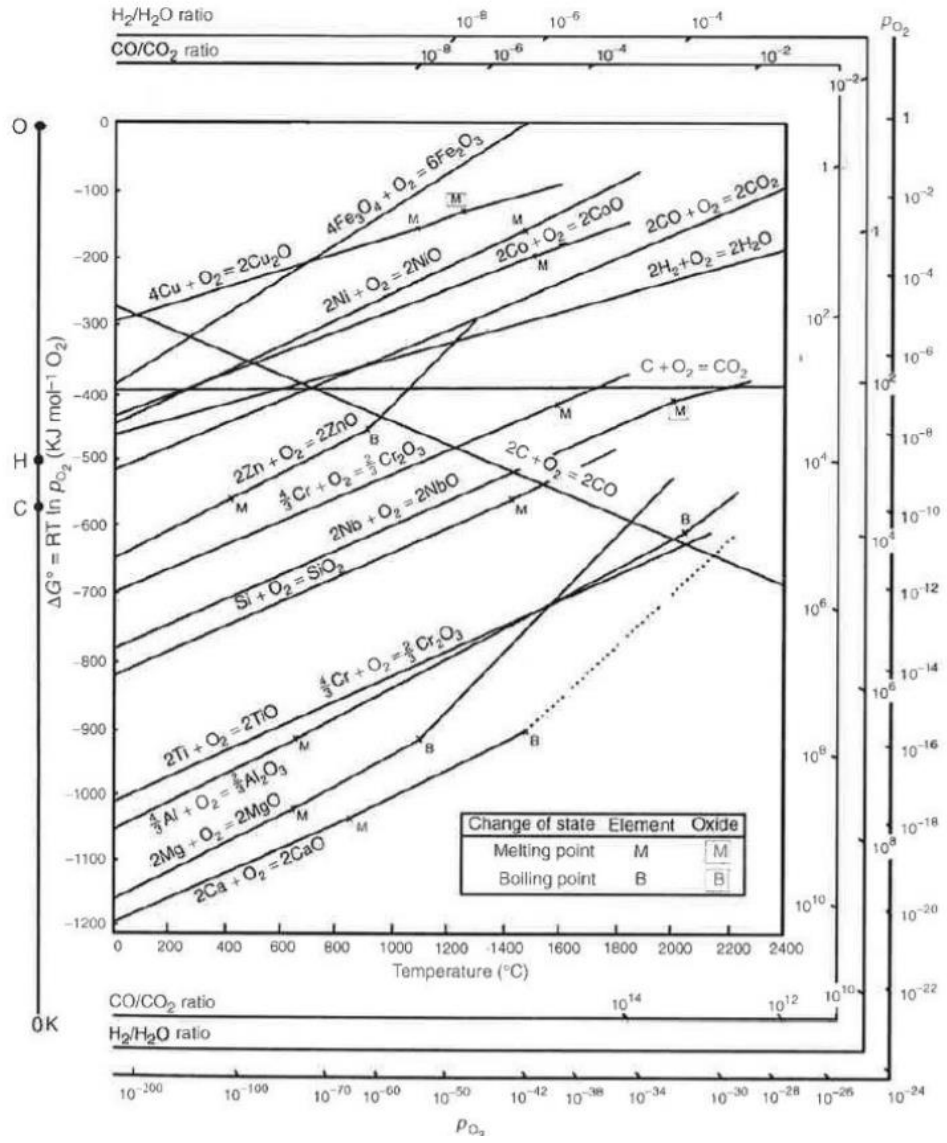

Figure 1. Picture of an Ellingham diagram [11].

The Ellingham diagram is obtained by plotting the enthalpy free energy on the y-axis and temperature on the x-axis, as can be seen in Caption 1. The lower the position of the metal line is, the more stable its oxide will be. The Ellingham diagram can thereby be used to predict which oxides form at different oxygen pressures.

Oxide formation

In general all metals oxidize while exposed to an oxidizing environment and the initial part of the oxidation can be described in three steps.

1) Adsorption and dissociation of the oxygen, where oxygen binds to the surface of the metal.
2) Formation of a thin layer of oxygen on the surface, as more oxygen binds to the metal.
3) Further growth of the oxide phase [12].

Kinetics

To measure the oxidation rate of a metal, various empirical rate laws can be applied. By plotting weight gained per unit area in function of time. These empirical rate laws can be estimated and calculated. There are three common rate laws which describe an oxidation rate: Linear, logarithmic and parabolic as can be seen in Figure 2. Although the oxidation rate generally depends on surface characteristics, temperature, elapsed time of reaction, gas composition and gas pressure. [13,14]

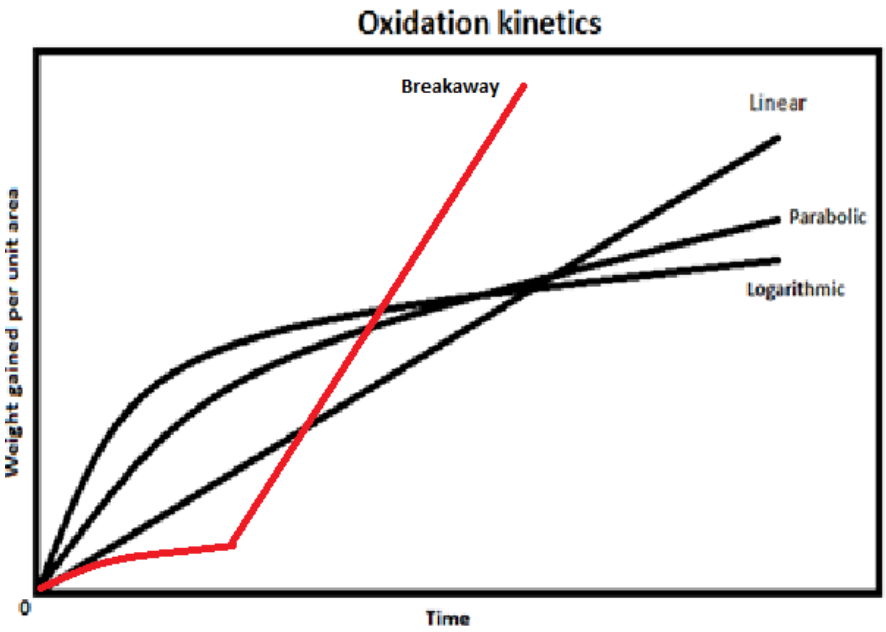

Figure 2. Linear, parabolic, logarithmic and breakaway rate law.

Linear rate law:

The linear rate law describes a system where the oxidation rate is constant and therefore exhibits a bad behavior toward corrosion. Linear rate behavior is typical for metals with cracked or porous oxide films and can be described by the following equation [14]:

Linear: x = kl * t + D [12]

Parabolic rate law:

Parabolic rate is typical for metals with a thick, continuous and even oxides, for example Cu and Fe [14]. To adapt the parabolic rate law diffusion of the metal cations and the oxygen anions is assumed to be the rate controlling variable. All other variables are assumed to be constant except the temperature which can be varied through the constant X according to the parabolic rate law formula [15]:

Parabolic: x^2 = kp * t + C [13]

Logarithmic rate law:

The logarithmic rate law is typical for oxidation in lower temperatures (< 400 C) and is rarely applicable in higher temperatures. The model can be used for thin layer oxidation of metals like Fe, Cu and Al. In a logarithmic behavior, the metal oxidizes at a fast rate from the beginning, and then the rate decreases to lower values over time [14]. The logarithmic rate law can be expressed as direct or indirect logarithmic as can be seen in the equations below:

Direct logarithmic: x = klog * log(t+t0) + A

Indirect logarithmic: 1/x = B - k * log t , [13]

It is not easy to adapt the oxidation rate of a metal to one of these laws and in many cases an oxidation behavior follows combinations of rate laws, as for example the breakaway oxidation curve. The combinations of rate laws can be a result of either two oxidation mechanisms taking place at the same time or changes during the oxidation process [13].

Potassium carbonate and potassium chloride

To improve the efficiency of biomass and waste fired boilers the steam temperature needs to be raised to around 500-600 °C, potentially reaching even higher temperatures. Increased efficiency of the boilers leads to a higher electricity output per emission of CO_2. Biomass and waste fired boilers can be run at lower temperatures of 450 °C without any great corrosion problems but at higher temperatures alkali salts accelerate the corrosion of the metal components inside the boiler [6][5]. Biomass and waste contains a low but relevant amount of potassium and chlorine, 0.05-2wt%. After combustion of biomass and waste, compounds such as KOH, K_2CO_3, KCl and K_2SO_4 are present in the flue gas. In combustion of fuel with low amounts of chlorine and sulfur, KOH and K_2CO_3 were present in the ash. The potassium containing compounds combined with the high temperature accelerate the corrosion of the super-heaters of the boiler. [16] The super-heaters are particularly targeted by the corrosion as the temperature in the boiler is at one of its highest points in the super-heaters. Also the

deposit layer on the heat exchangers consists of ash from burnt biofuel leading to contact with the alkali salts in the ash. [6][17]

At temperatures of 500-700 °C chlorine and potassium are released from the fuel during combustion and reacts to form alkaline salts, mostly KCl and NaCl. During the heating and cooling process of the boiler, chlorine is formed when alkali salts reacts with sulfur dioxide.

To withstand corrosion at high temperatures stainless steel alloys depends on the formation of a chromia layer. [6] At high temperatures in an O_2/H_2O environment the chromia layer reacts with water and oxygen to form chromium hydroxide.

(2) ½ Cr_2O_3 (s) +H_2O (g) + ¾ O_2 (g) → $CrO_2(OH)_2$

The breakdown of the chromium oxide in the boiler is further accelerated by the formation of potassium chromate. Potassium chloride reacts with the protective oxide in an H_2O/O_2 environment to form potassium chromate and hydrogen chloride.

(3) ½ Cr_2O_3 (s) + 2 KCl (s) +H_2O (g) + ¾ O_2 (g) → K_2CrO_4 (s) + 2 HCl (g)

After the depletion of the chromium from the protective oxide layer, chlorine molecules and ions can diffuse through the oxide scale and cause active oxidation. [6][18] The chlorine reacts with the metal at the metal/oxide interface creating highly volatile metal chlorides.

(4) Fe (s) + Cl_2 (g) → $FeCl_2$ (g)

The metal chlorides then diffuses back to the surface of the oxide scale. The high oxygen partial pressure outside of the scale prompts the metal chlorides to dissociate. The metal ion then reacts with oxygen, forming metal oxide. The chlorine ion released from the metal can diffuse through the oxide layer again and restart the mechanism from (2).

(5) 2 $FeCl_2$ (g) + 3/2 O_2 (g) → Fe_2O_3 (g) + 2Cl_2 (g)

This phenomenon means the chlorine catalyzes the reaction of metal being transported from the structure, leading to corrosion of the metal. [18] [8]

The chloride however can react with water as the combustion vapor contains up to 25 % water, see reaction (6). This reaction is although only favorable if the oxygen activity is high and the chloride ions are not allowed to diffuse through the oxide. The oxide scale is impermeable to molecular oxygen. It is assumed that the chlorine ions have a high activity inside the boiler which means reaction (6) is not favored. [6]

(6) $H_2O\ (g) + Cl_2\ (g) \rightarrow 2\ HCl\ (g)$

Primary protection

In most environments at high temperatures most metals are thermodynamically unstable and convert to oxides. [7] To protect the metals from corroding the formation of oxide is supposed to be at a sufficiently low rate so that the lifespan of the metal is acceptable. The metal can be protected through formation of a continuous and slow growing oxide scale over the metal. Which serves as a barrier from further oxidation by keeping the metal and oxygen diffusion at low rates. Austenitic stainless steel creates different protective oxide scales depending on the elemental composition of the steel. [19][20] Choosing elemental composition comes with a need to balance several different properties. Corrosion resistant metals used in a biomass- and waste fired boiler still has to maintain high temperature strength and toughness. Generally adding nickel as a stabilizing agent enhances the mechanical properties of stainless steels by stabilizing the austenitic structure, which otherwise is not stable at room temperature. [21] High nickel alloyed steels are often used in corrosive environments as nickel also has effective protective properties towards certain acidic compounds. Stainless steels contains chromium to provide up to 900 °C corrosion resistance. At least 12% of chromium is required to obtain a stainless steel. [22][23] Stainless steels oxidation stages, the primary and the secondary protection.

The primary protection is a protective oxide growing inwards consisting of tightly packed chromia $(Fe, Cr)_2O_3$ particles and a compact layer of nano-sized spinel oxides. The close packed structure gives the inner oxide protective properties, preventing active corrosion of the metal. [19][24] Cr_2O_3 scales are protective up to 900 °C. However presence of alkali compounds or water vapor in the environment surrounding the metal can significantly reduce the corrosion resistance. The alloy also has to form a coherent oxide scale to avoid corrosion attacks at specific locations. [20] [7] The elemental composition in the spinel group being $(Ni, Fe, Cr)_3O_4$.

Breakaway oxidation

As mentioned before, chromium commonly oxidizes as Cr_2O_3 which creates a thin protective oxide layer on the alloy surface. However, at longer exposures and in specific environments, the chromia tends to break down which results in an increased oxidation rate. This is called breakaway corrosion [25].

Breakaway corrosion during exposure of water vapor

Chromia forming steels, like for example 304L, relies on the formation of chromium rich oxide to protect the surface from corrosion. The oxidation rate gets considerable lower in temperatures around 400-600°C after the initial oxidation in a dry oxygen environment. However, in an environment containing oxygen and water vapor, the alloy experiences an accelerated oxidation. High concentrations of water vapor and high flow rates has been reported to result in a mass gain of about four to five times greater than oxidation in dry O_2 during a 168h exposure [26]. While being exposed to water, the chromia tends to react with the water and form chromic acid ($CrO_2(OH)_2$) which depletes the Cr of the protective layer. Once the protective layer has depleted, iron oxide and nickel oxide starts to form which results in a much higher growth rate.

Breakaway corrosion during exposure of KCl and K_2CO_3

During exposure of KCl and K_2CO_3 the salt in addition to O_2 and H_2O reacts with the primary protective chromia oxide to form K_2CrO_4, according to reaction 7 and 8, and thereby depletes the chromium. Once the potassium has bonded to the oxide, the remaining products HCl and CO_2 leaves the furnace along with the gas flow [6].

(7) $\frac{1}{2}\ Cr_2O_3\ (s) + 2\ KCl\ (s) + H_2O\ (g) + \frac{3}{4}\ O_2\ (g) <-> K_2CrO_4\ (s) + 2\ HCl\ (g)$

(8) $\frac{1}{2}\ Cr_2O_3\ (s) + K_2CO_3\ (s) + \frac{3}{4}\ O_2\ (g) <-> K_2CrO_4\ (s) + CO_2\ (g)$ [6]

Secondary protection

After depletion of the primary protective mechanism or if the conditions promote it, iron oxide starts growing outwards. Which oxides that form and at what rate depends on elemental composition, partial pressure and environment surrounding the metal. This oxidation stage is defined as the secondary protection. The secondary oxide is a fast growing oxide and have poor protecting properties, it works as a protective oxide only in low temperatures. At high temperatures the oxide allows high diffusion rates of metal and oxygen ions. This leads to an increase of mass gain, loss of metal from the structure and can open micro cracks in the structure. The secondary oxide consists of non-stoichiometric hematite structure, Fe_2O_3, and loosely structured spinel groups. The elemental composition in the spinel group being $(Ni, Fe, Cr)_3O_4$. [19][24]

Grain size

Corrosion of a metal is selective towards a certain part of the metals microstructure. This can lead to uneven oxidation of the metal if the surface is not homogenous. The microstructure of the metal consists of several grains, varying in size. Grain boundaries have distinct properties relative to the bulk material. As the electrochemical properties can vary at the grain boundaries the corrosion mechanism might alter depending on the shape and size of the grains. Metals often undergo heat treatment to improve microstructural properties or creating a homogenous material. [27] For stainless steels a decrease in grain size leads to lower/higher oxidation rates depending on the environment. [28] [29] Active corrosion is more prone to occur if the grain size is small. Small grain size leads to more grain boundaries which means ions has more easily diffuse through. Thickness of grain boundaries and grain size affects the mass transport for the formation of oxide. In an environment where passivity could be established, small grain sizes tend to improve the corrosion resistance of the metal.

Analyzing methods

During oxidation the performance of the metal often depends on the protection of the formed oxides on the surface. Therefore, it is important to know the structure of the oxide surface to be able to analyze the growth rate and which oxides are formed. Using different analyzing techniques, one can thereby analyze and use different surface properties to predict the formed oxide and its growth rate [30].

There are many kinds of analyzing techniques with different sensitivity, methods and results. A combination of these analyzing techniques are often used to determine the corrosion behavior of the alloys but in this report, the main focus will be on SEM/EDX (Scanning Electron Microscopy and Energy Dispersive X-ray) and BIB (Broad Ion-Beam).

Scanning Electron Microscopy

SEM is an analytic instrument used to analyze the surface of the alloy and its composition. It scans the surface of the alloy by using a beam of high energy electrons, which will interact with the atoms of the sample. The interactions between the electrons and the sample give information like chemical composition and surface morphology. The data are most commonly collected from a selected area of the surface and images of the sample can be taken for further analysis and comparison. The SEM can also perform EDX analysis of selected points for quantitative information about specific parts of the surface [31][32].

The SEM mainly consists of six essential components:

- An electron source
- Electron lenses
- Sample stage
- A detector which detects the signals of interest
- Display/ computer which interprets the data
- Infrastructure requirements [31]

Broad Ion Beam

Broad ion beam (BIB) is a sample preparation technique used to prepare the cross section of a sample for the SEM. The samples are first cut in half to expose the cross section for the BIB. The BIB then uses a beam of ions, in this case argon ions, to mill the samples [33]. A titanium mask is used to protect the sample surfaces and only the cross section are exposed during the milling [34]. This milling process polishes the sample edge and a clear even surface is achieved and facilitates a more detailed analysis using the SEM [33].

Experimental

Polishing:

For accurate and reliable results all samples of metal alloys has to be polished. The surface of the samples that was used had the measurements of about 1 x 1 cm with a depth of 2 mm. The polishing was done on the edges and the surface with the use of abrasive grinding paper and two different rotating grinding machines.

For the edges polishing was done with a Struers RotoPol-31 with the use of silicon carbide paper (SiC). All the edges were polished to a round shape. SiC paper 1000 was used and the sample was held against the rotating paper for about 10-15 seconds per side. Water was used as lubricant for the procedure.

For surface polishing the samples were fastened on a rotating shaft with double sided tape. Eight samples were fastened at a time as symmetrical as possible. The rotating shaft was then fastened in a Struers TegraPol-31 device. The machine is automatic and polishes for a designated time. After each step the rotating shaft and samples were cleaned with distilled water. The program used consist of four steps. The first step was 3 minutes of polishing with SiC paper 500, using water as lubricant. For the next 3 steps the lubricant used was Dp-lubricant yellow. The samples were cleaned and the rotating shaft was fastened again and polished by 9 µm Largo paper for 4 minutes, only lubricant used. For the last two steps a suspension was also used. After cleaning the samples they were polished with 3 µm Dac. The polishing was done for 4 minutes with the same lubricant and Dp-suspension A 3 µm. The samples were thereafter cleaned again and polished for 3 minutes using Dp-suspension A 1µm and Dp-lubricant yellow.

After the polishing was complete the samples were carefully removed and fastened with the polished side downwards. The polishing procedure was then repeated on the other side of the samples.

When both sides of the samples had been polished the samples were cleaned with acetone and ethanol in an ultrasonic bath. The ultrasonic bath was set at around 60 degrees Celsius and at a frequency of 80 Hz. The samples were put in plastic tubes with a covering cap. First the tubes were filled with acetone so that the entire sample was covered with acetone. The tubes were placed in the ultrasonic bath for 15 minutes. The samples were then removed carefully and the tubes emptied before being filled with ethanol so that the samples were covered and again put in the ultrasonic bath for 15 minutes.

When the samples were cleaned and polished they were put in a plastic holder until further testing.

Depositing the salts:

A hole was drilled in the samples used for K_2CO_3 and KCl exposure before the polishing. Once the samples have been polished they were hung on a hook and placed in a desiccator for further pre exposure treatment.

The sample hooks were weighed to be able to calculate the weight of the sprayed samples. Each sample were then weighed using a sensitive scale and the dimensions were measured to be able to calculate a total area and weight of the sample. The sprayed samples were weighed with their hook and the samples which were not sprayed were weighed without a hook.

Once all measurements had been written down and calculated the samples were sprayed with saturated K_2CO_3 and KCl solutions using nitrogen as carrier gas. Each sample was sprayed with an amount of about 1 mg/cm^2, subsequently weighing the sample to ensure that the right amount was applied. During the spraying a hairdryer were used to quickly dry the salt solution and obtain a homogeneous salt layer on the sample surfaces. Thereafter the samples were placed back in the desiccator until furnace exposure.

Exposure of the samples:

The exposure of the samples were performed using a horizontal tube furnace.

The samples were placed in a sample holder, however some samples were too thin to fit into the holder and therefore golden foil pieces were used to fill the gap and make the samples fit into the holder. Once the samples had been carefully placed in the holder, the relevant parameters for the exposure were checked. The temperature inside the furnace was calibrated at 600 +- 2 °C using a thermocouple. Thereafter to gas flows were calibrated using a Bios Definer 220M. The water flow were calibrated using a tempered water bath which was manually refilled. Once the environment had been checked the samples were inserted into the furnace.

After the samples had been pushed into the middle of the furnace, the entrance tube was sealed. The flow of gas and water were calibrated to be (1) 20% H_2O + 5% O_2 + N_2 (bal.) for the non-sprayed and KCl alloys and the sample sprayed with K_2CO_3 were exposed without water. The samples were then left in the furnace for 24 hours in a stable environment.

After approximately 24 hours the exposure were finished and the samples were taken out of the furnace and were then weighed again to be able to calculate mass gain.

Analysis of the samples:

After exposure was done analyzing of the samples were done with SEM (scanning electron microscopy). To prepare the samples for SEM they have to be cut in half and the cross section smoothen.

To be cut a small silica waifer piece was glued on top of the sample with Loctite 415 glue. The samples was then let to dry inside of a plastic container for 24 hours. Samples exposed to KCL were stored in airtight plastic holder. Samples were then cut at the middle of the silica waifer piece by a Struers Minitom saw with a 0.3 mm thick blade. The samples were then polished with SiC 500 paper until the cross section was even. The cut samples were then run in a BIB (broad ion beam) for 12 hours to get a smooth surface.

After the preparation the samples were analyzed in a scanning electron microscope. For analyze pictures of surface and cross section was done with appropriate holders. Pictures of surface and cross section was taken for all samples. Mapping and point analysis was done to determine compositions at different locations.

Results

Three different alloys with the following compositions were tested regarding their corrosion resistance in different environments. The compositions of the alloys can be seen in table 1.

Nickel

Löpnr.	Cr	Ni	Al
11	18	20	*
12	18	34	*
13	18	Bal.	*

* < 0.01 wt%

Table 1. Alloys used were 11, 12 and 13.

A background test was run with 5% O_2 for 24 hours. The result can be seen in graph 1. The alloy with 34 wt% nickel showed the highest mass gain and the 20 wt% alloy showed the smallest mass gain of the samples.

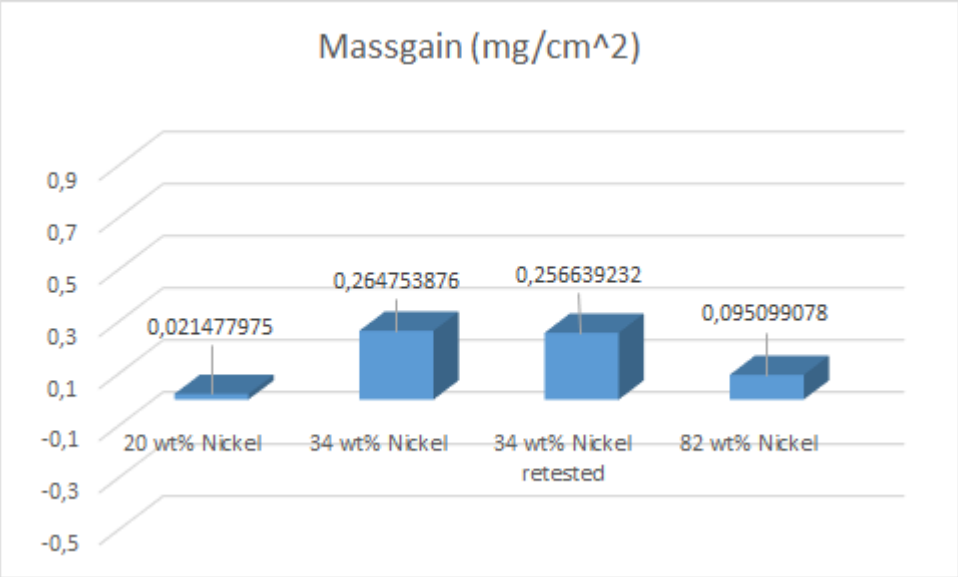

Graph 1. Mass gain after 5% O_2 + bal. N_2 exposure.

Exposure to N_2, H_2O and 5% O_2.

For the first exposure of N_2 and air for 24 hours, 3 samples of each alloy were selected and evaluated for mass gain results. The mass gains for the different alloys can be seen in graph 2.

Weighing after exposure showed that the alloy with 34 wt% nickel had a much higher mass gain relative to the other samples. The relative mass gain is visualized in graph 2.

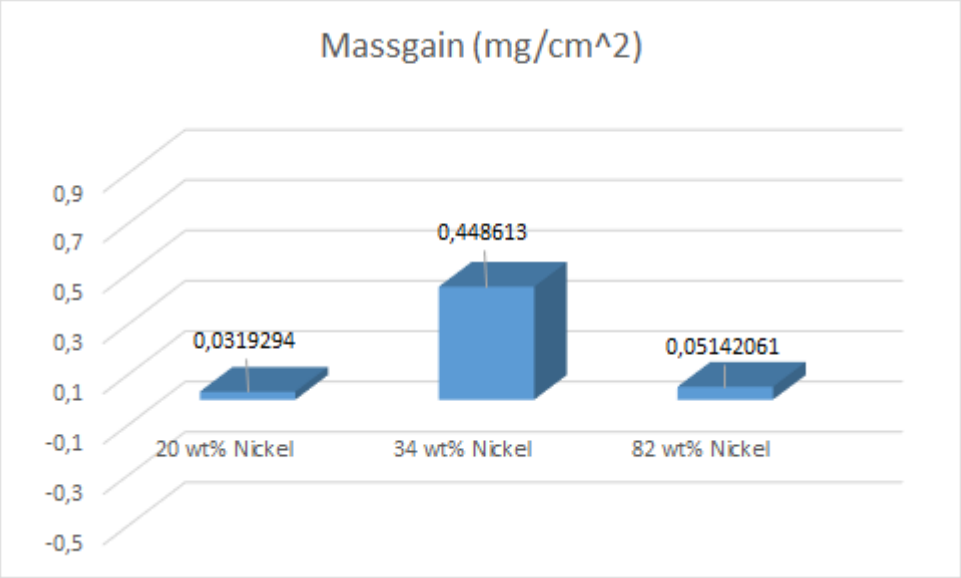

Graph 2. Mass gain after H_2O + 5% O_2 + bal. N_2 exposure.

The mass gain is related to the oxide growth. An increase in mass gain from one sample to another could mean more growth of oxide on the sample surfaces. The oxide growth of two samples of each alloy were analyzed with SEM. One sample was investigated on the surface while the other one at the cross section.

From the mass gain of the samples, a theoretical oxide thickness could be calculated. This calculation is done by dividing the mass gain (mg/cm^2) with the molar fraction of oxygen in the oxide times the density of the oxide. The equation can be seen in (9).

(9) $T = \Delta m/(\rho*(n*M_O/M_{tot}))$

The equation is a simplification of the reality of the oxide and is based on the presumption that only one type of oxide grows from the metal as well as that no evaporations of the salt takes place. Based on the mapping done with SEM the dominating oxide is used for calculations. For an iron oxide the assumption is made that the oxide is of hematite (Fe_2O_3) structure. The molar fraction of oxygen relative to the entire compound is 0.3, which will be used in calculations. For nickel oxide (NiO) the molar fraction is 0.21. The density for the two oxides is 5.24 g/cm^3 for iron oxide and 6.67 g/cm^3.

The result of the calculations for the thickness of the oxides can be seen in table 2.

Exposure	20 wt% nickel (µm)	34 wt% nickel (µm)	82% nickel (µm)
5% Oxygen	0,136363	1,655162	0,665593
Oxygen and water	0.202719	2.848240	0.508662
Oxygen and K2CO3	1.815839	1.489230	-
Oxygen, water and KCl	5.325654	3.480435	-

Table 2. Calculated oxide thickness in µm.

Alloy 11 water exposure

The alloy containing 20 wt% nickel which showed the least amount of mass gain also showed a discontinuous layer of oxide. The oxide formed as crusts dispersed on the surface but no continuous layer. In figure 3 the cross section of the sample can be seen and shows two oxides, one growing outwards and the other inwards. Figure 4 of the surface showed oxide fragments almost growing at random in no particular pattern.

Point analysis (figure 5) revealed that the oxide growing outwards contained chromium and iron oxide while the inward growing oxide also contained nickel oxide.

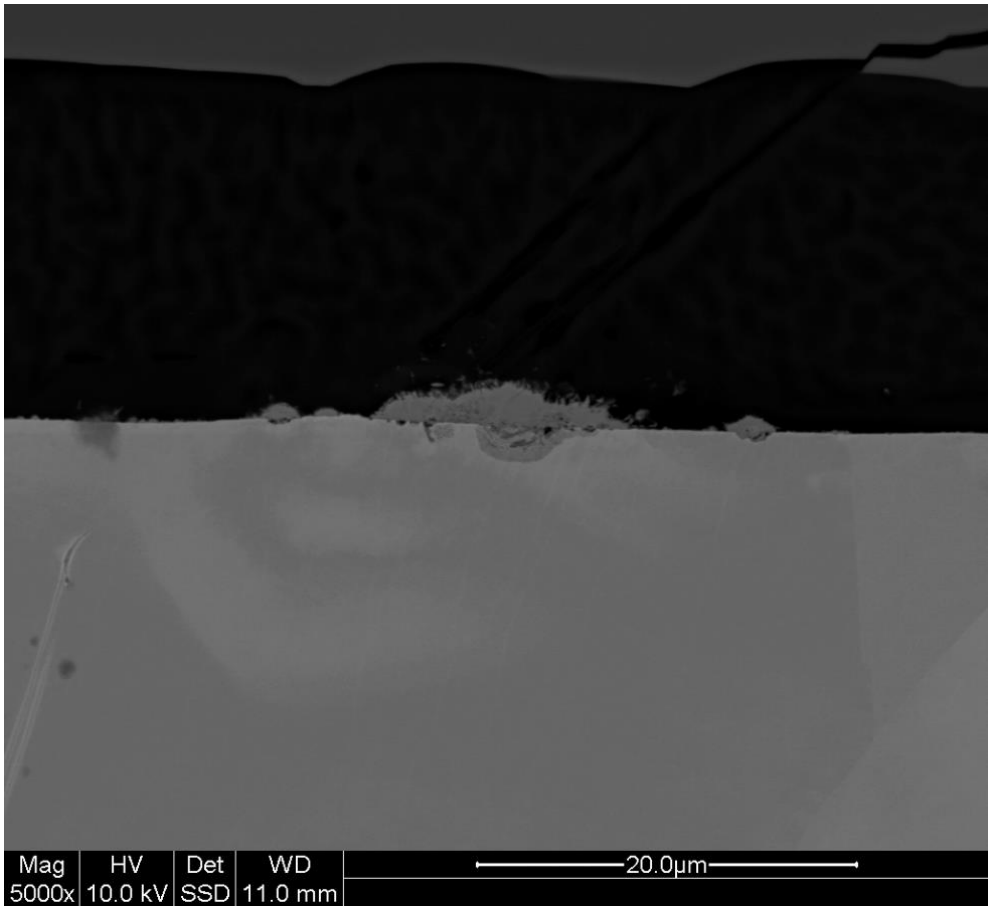

Figure 3. Cross section of 20 wt% nickel exposed to H_2O, N_2 and 5% O_2.

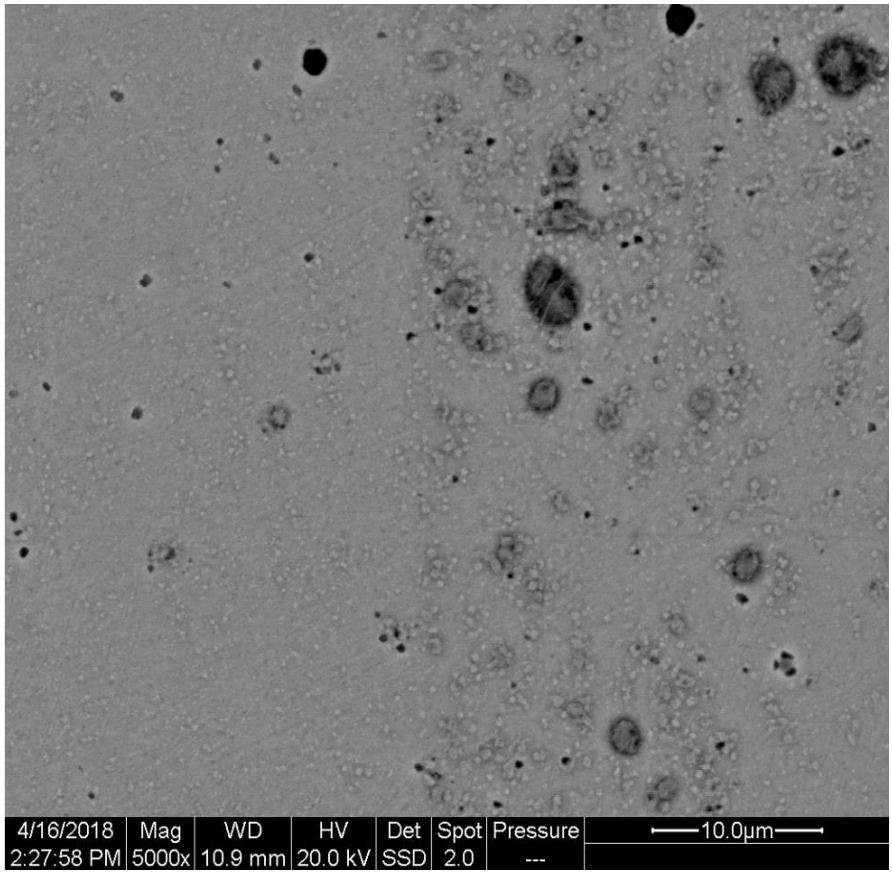

Figure 4. Surface picture of 20 wt% nickel exposed to H_2O, N_2 and 5% O_2..

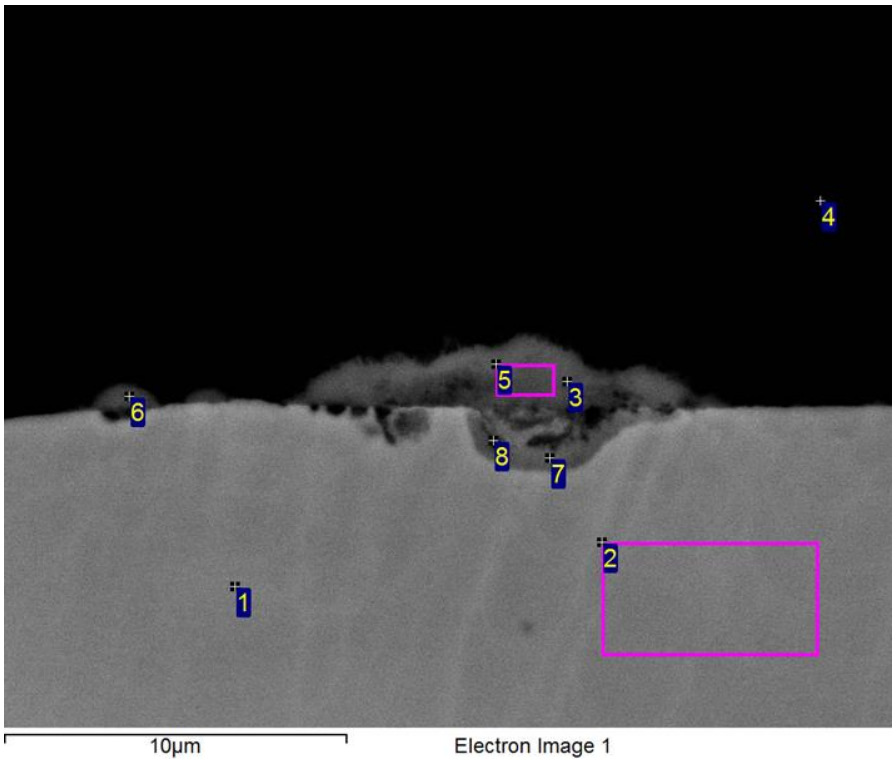

Figure 5. Point analysis cross section of 20 wt% nickel exposed to H_2O, N_2 and 5% O_2.

Spectrum	In stats.	O	Cr	Fe	Ni
1	Yes	1	19	62	18
2	Yes	1	19	62	18
3	Yes	53	19	27	1
4	Yes	97	1	2	0
5	Yes	54	16	28	1
6	Yes	51	18	29	3
7	Yes	35	20	25	21
8	Yes	35	26	24	16

Table 3. Point analysis of 20 wt% nickel exposed to H_2O, N_2 and 5% O_2.

Alloy 12 water exposure

The alloy containing 34 wt% nickel had the highest mass gain of the three alloys after being exposed to H_2O, O_2 and N_2. The mass gain was 9 times bigger than the one of the alloy with 20 wt% nickel. The oxide spread continuously across the surface but had reduced oxide growth at the grain boundaries, as can be observed in figure 7. In the cross section different oxide phases can be spotted and both inwards and outwards growing oxide is observed. The point analysis seen in figure 8 and table 4 showed that the oxide growing outwards consisted of iron and nickel oxide. The inwards growing oxide contained same composition of nickel and chromium as the bulk material but depletion of iron can be observed, therefore a mix of all three oxides are likely to grow. However, the outwards growing oxide consisted of two visible oxide phases, see figure 6. Observing the two phases using point analysis, see Figure 8, the outer phase seems to consist of mostly iron oxide. In the inner phase the nickel content was higher and therefore a mix of both iron and nickel oxide should be present. Barely any chromium was detected in any of the two phases of the outwards growing oxide.

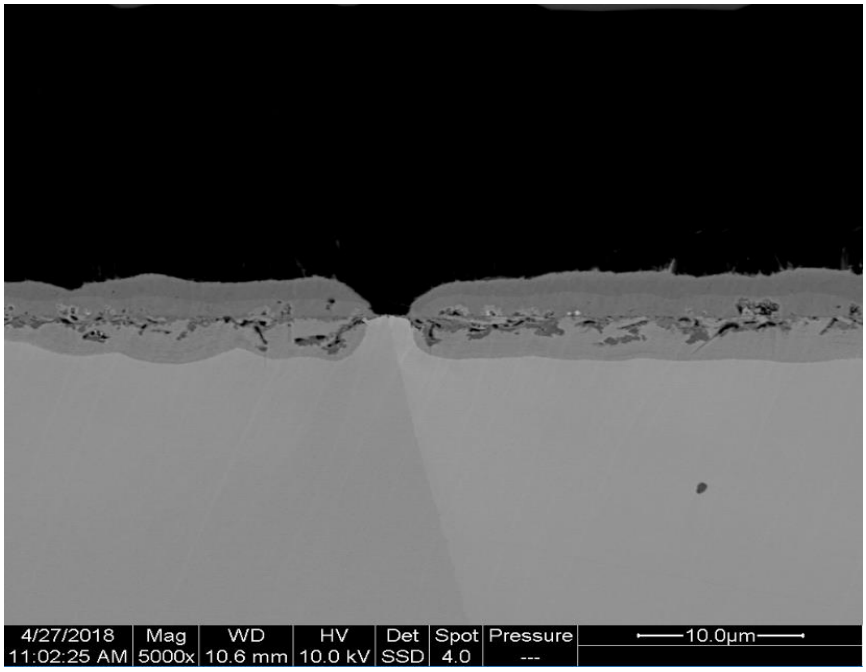

Figure 6. Cross section of 34 wt% nickel exposed to H_2O, N_2 and 5% O_2.

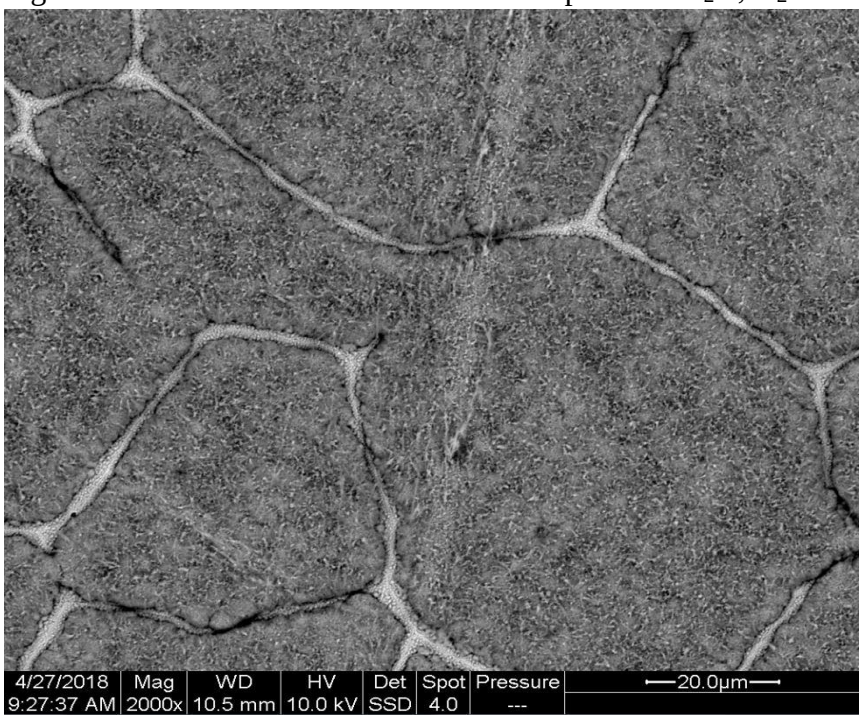

Figure 7. Surface picture of 34 wt% nickel exposed to H_2O, N_2 and 5% O_2.

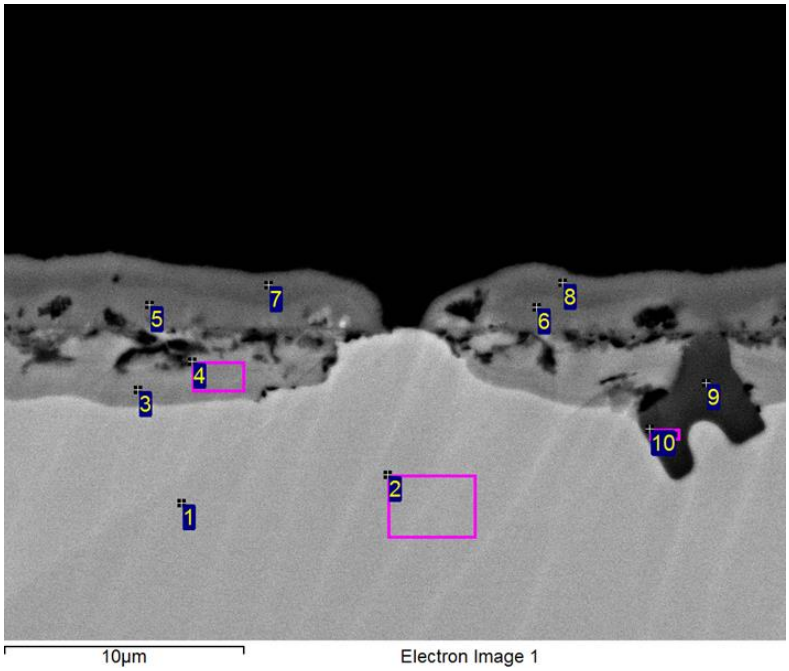

Figure 8. Point analysis of 34 wt% nickel exposed to H_2O, N_2 and 5% O_2.

Spectrum	In stats.	O	Cr	Fe	Ni
1	Yes	1	20	48	32
2	Yes	1	19	48	31
3	Yes	37	18	14	31
4	Yes	38	18	13	31
5	Yes	55	1	30	14
6	Yes	55	2	31	12
7	Yes	57	1	41	1
8	Yes	58	1	40	1

9	Yes	59	40	1	0
10	Yes	55	39	4	2

Table 4. Point analysis of 34 wt% nickel exposed to H_2O, N_2 and 5% O_2.

Alloy 13 water exposure

The alloy containing 82 wt% nickel had a slightly higher mass gain than the 20 wt% nickel one and had a thin continuous oxide layer. The thin layer could be observed in both the cross section in figure 9 and the surface picture in figure 10. Observing the cross section a thin layer of oxide spread continuously across the surface can be seen and although it is thin, there is both inwards and outwards growing oxide. The cross section also revealed clear grain boundary attacks where the oxide had grown along the grain boundaries into the alloy.

Point analysis (figure 11) revealed that the outward growing oxide had less chromium than the bulk material and consisted of a mix of chromia and mainly nickel oxide. It also showed that the grain boundary attacks had chromium enrichments.

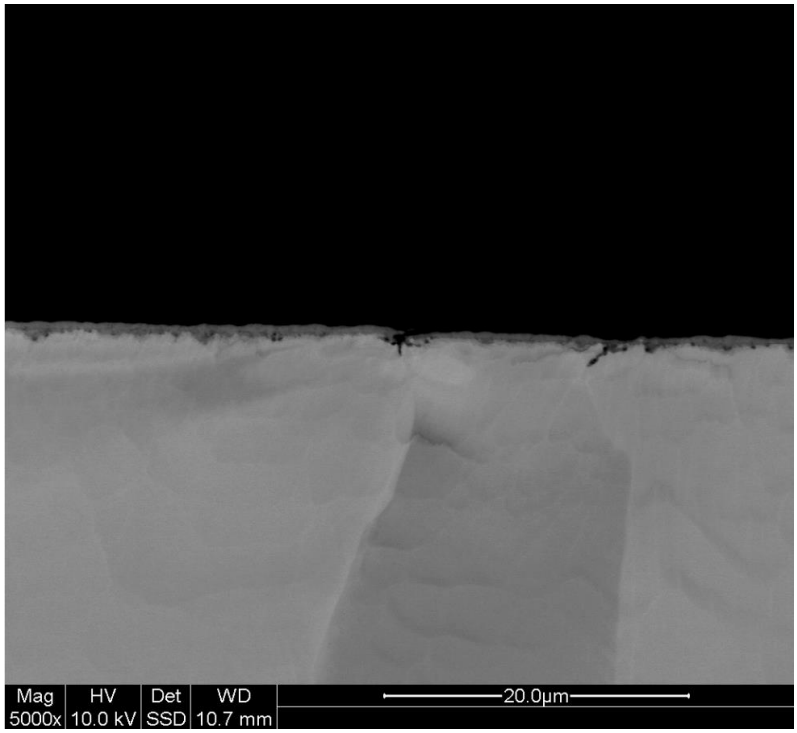

Figure 9. Cross section of 82 wt% nickel exposed to H_2O, N_2 and 5% O_2.

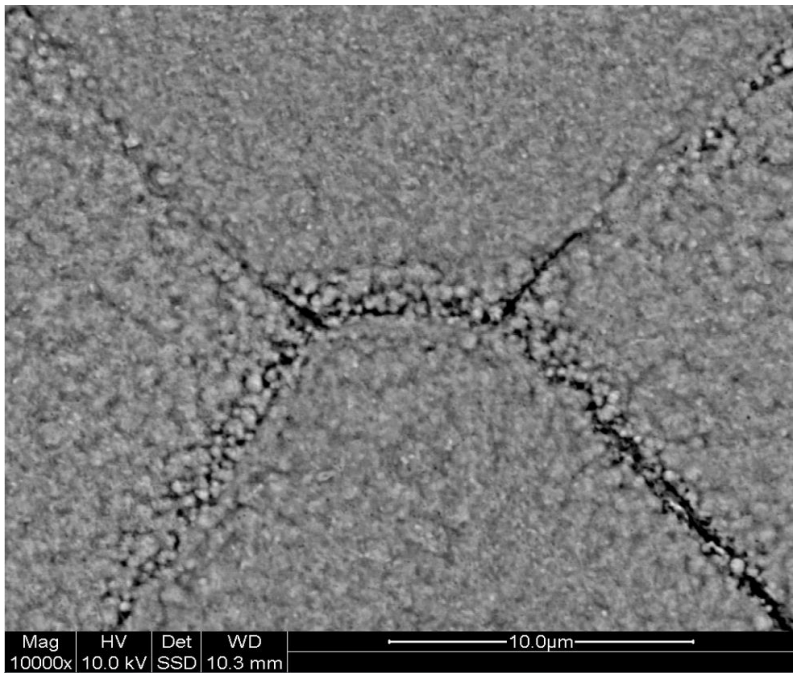

Figure 10. Surface picture of 82 wt% nickel exposed to H_2O, N_2 and 5% O_2.

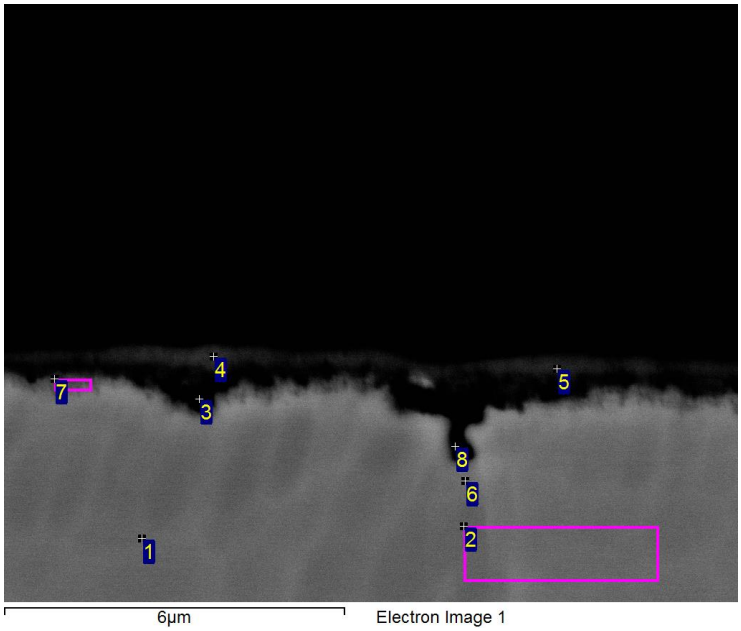

Figure 11. Point analysis of 82 wt% nickel exposed to H_2O, N_2 and 5% O_2.

Spectrum	In stats.	O	Cr	Fe	Ni
1	Yes	1	19	1	79
2	Yes	1	19	1	79
3	Yes	31	22	1	46
4	Yes	46	7	0	47
5	Yes	44	9	1	46
6	Yes	3	10	1	87
7	Yes	26	18	0	56
8	Yes	19	25	1	55

Table 5. Point analysis of 82 wt% nickel exposed to H_2O, N_2 and 5% O_2.

K_2CO_3 exposure with oxygen

The alloy with 20 wt% nickel showed the biggest mass gain when exposed to potassium carbonate (K_2CO_3) as can be seen in graph 3. The mass gain of this alloy increased by a factor of 6 compared to the exposure without potassium carbonate. The 34 wt% nickel showed a decrease in mass gain compared to the exposure without potassium carbonate. The alloy with 82 wt% nickel showed both mass gains and mass losses. The exposure was redone two more times on new samples but the mass difference differed between a mass gain of 0.29 mg and a mass loss of 0.46 mg as can be seen in table 6. The mass loss was almost half of the total sprayed amount, probably meaning some sprayed K_2CO_3 evaporated during exposure.

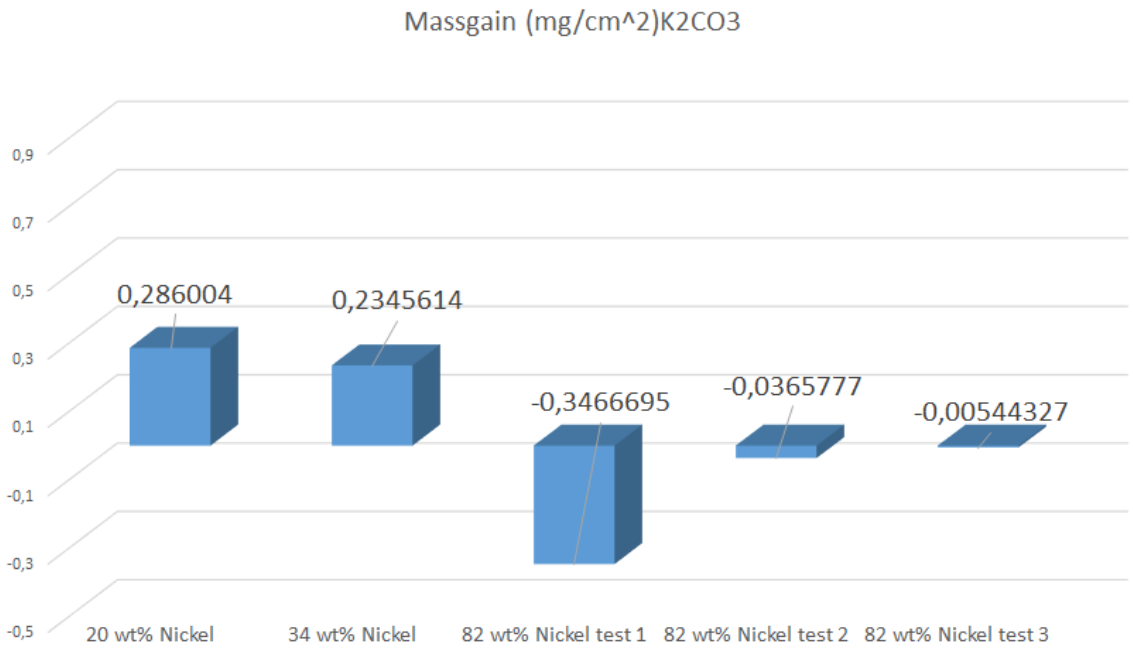

Graph 3. Mass gain after exposure to K_2CO_3 and N_2 and 5% O_2.

82 wt % nickel exposed to K2CO3:	Mass gain results:
Sample 1	-0.463622
Sample 2	-0.229716
Sample 3	-0.327516
Sample 4	0.290939
Sample 5	-0.031899
Sample 6	0.026455

Table 6. Mass gain for alloy 13 with 82 wt% nickel exposed to H_2O, N_2 and 5% O_2.

Alloy 11 K_2CO_3 exposure

The alloy with 20 wt% nickel showed the highest mass gain of the K_2CO_3 samples. As can be seen in figure 12 the surface differs between the bulk material and the grain boundaries. The mapping seen in figure 13 shows iron oxide growing on the grains. Chromium and nickel enrichments are seen at the grain boundaries but the oxide layer at the boundaries are very thin indicating that there is probably mainly chromium oxide formation at the grain boundaries.

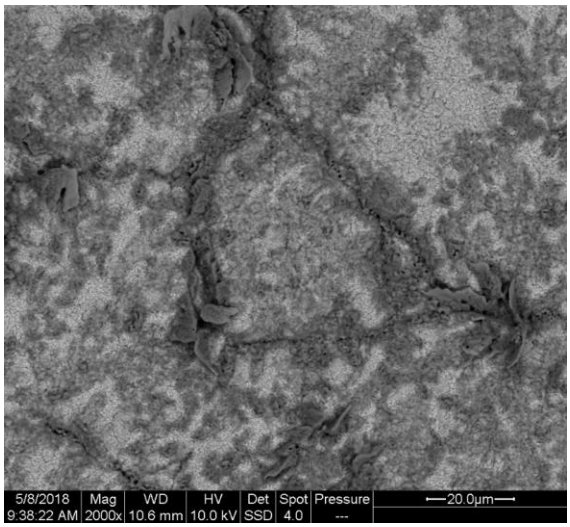

Figure 12. Surface picture of 20 wt% nickel exposed with K_2CO_3, N_2 and 5% O_2.

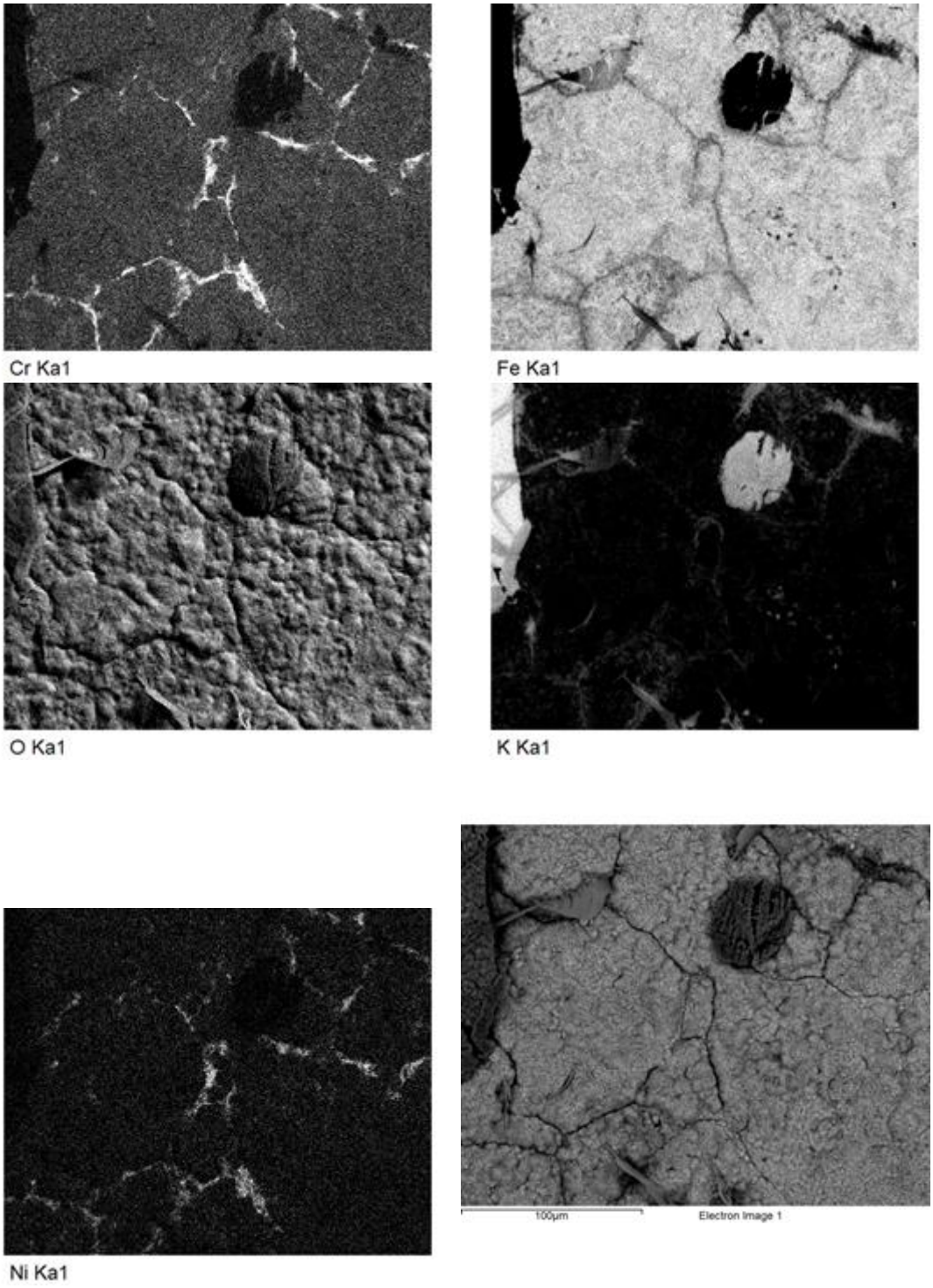

Figure 13. Surface mapping of 20 wt% nickel exposed to K_2CO_3, N_2 and 5% O_2.

Alloy 12 K_2CO_3 exposure

The alloy which contained 34 wt% nickel showed about the same mass gain as the samples exposed to water and air. As can be seen in figure 15 and 16 an iron oxide grows on areas that isn't covered by potassium carbonate. There seems to be less oxide at the grain boundaries where more nickel and chromium is present, probably in metal state.

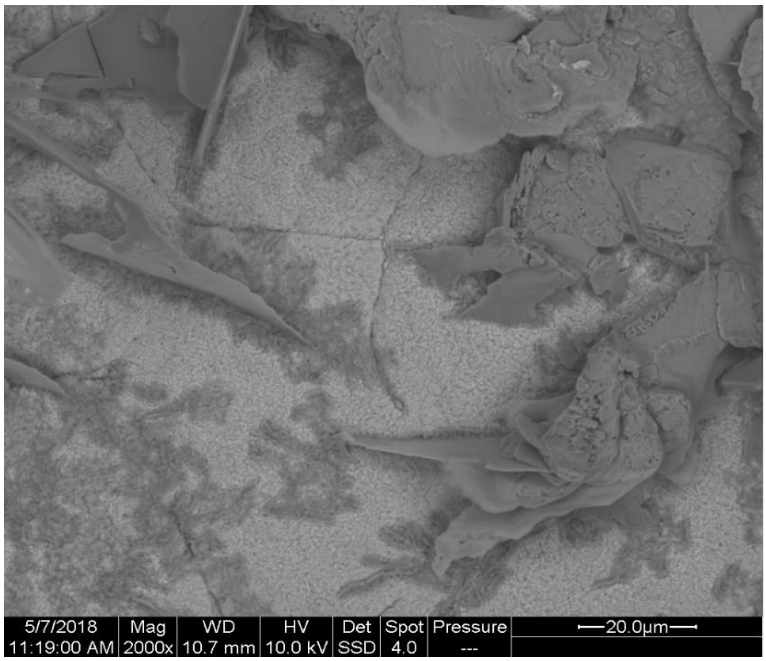

Figure 14. Surface picture of 34 wt% nickel exposed to K_2CO_3, N_2 and 5% O_2.

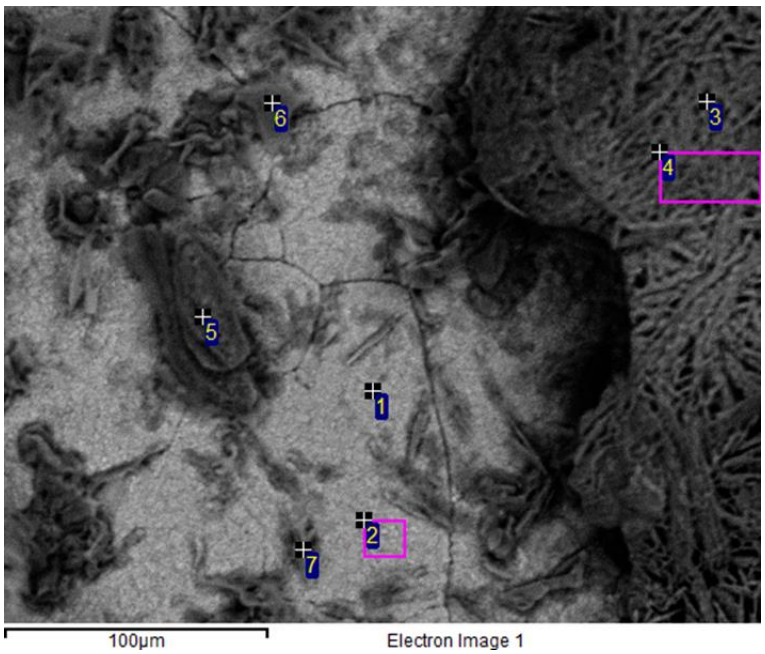

Figure 15. Point analysis 34 wt% nickel exposed to K_2CO_3, N_2 and 5% O_2.

Spectrum	In stats.	C	O	K	Cr	Fe	Ni
1	Yes	14	45	2	1	37	0
2	Yes	15	49	3	1	32	0
3	Yes	27	55	18	0	0	0
4	Yes	27	56	18	0	0	0
5	Yes	23	49	28	0	0	0
6	Yes	31	46	15	0	8	0
7	Yes	28	52	8	0	12	0

Table 7. Point analysis 34 wt% nickel exposed to K_2CO_3, N_2 and 5% O_2.

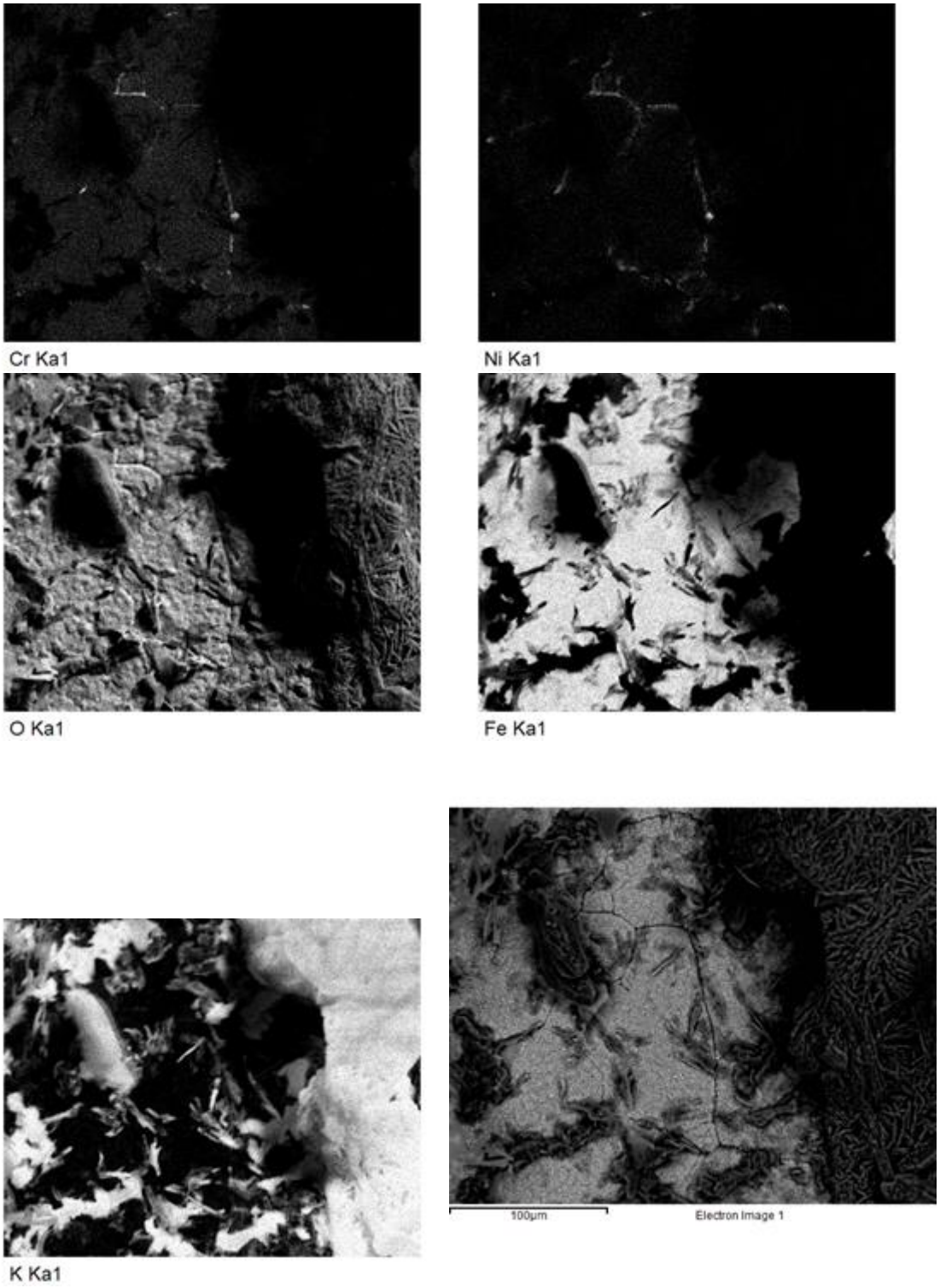

Figure 16. Surface mapping of 34 wt% nickel exposed to K_2CO_3, N_2 and 5% O_2.

Alloy 13 K_2CO_3 exposure

The alloy containing 82 wt% nickel had an unexpected mass gain which was mostly negative, but altered a lot. The mapping pictures in Figure 19 shows that the oxide seems to grow around bigger accumulations of K_2CO_3. There is also a very low activity of chromium and potassium mixes on the surface, build ups of potassium can be seen clearly. The mass loss is probably due to K_2CO_3 evaporating from the surface before affecting the metal. The growing oxide seems to be a mix of chromium- and nickel oxide with the majority of the oxide containing nickel, as can be seen in figure 18 and table 8.

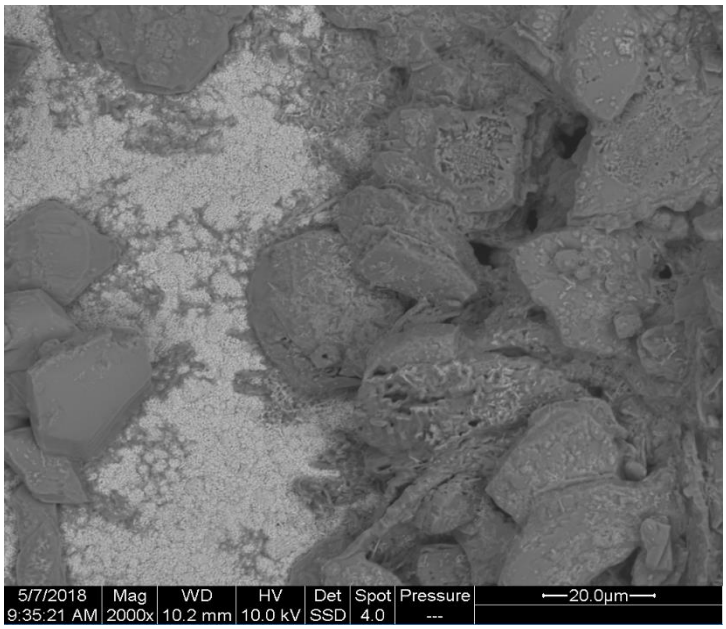

Figure 17. Surface picture of 82 wt% nickel exposed to K_2CO_3, N_2 and 5% O_2.

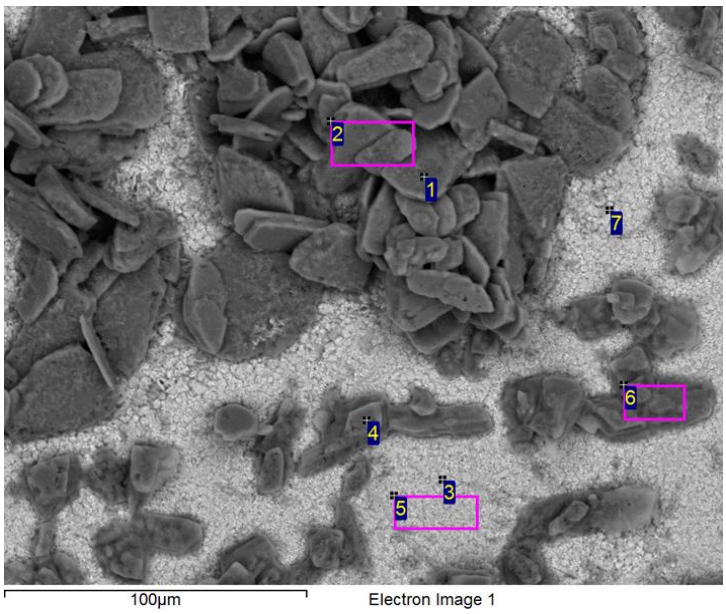

Figure 18. Point analysis of 82 wt% nickel exposed to K_2CO_3, N_2 and 5% O_2.

Spectrum	In stats.	C	O	K	Cr	Ni
1	Yes	26	49	25	0	1
2	Yes	21	51	27	0	1
3	Yes	16	39	2	3	40
4	Yes	21	46	32	0	1
5	Yes	14	41	2	3	40
6	Yes	26	53	20	0	1
7	Yes	29	28	3	3	37

Table 8. Point analysis of 82 wt% nickel exposed to K_2CO_3, N_2 and 5% O_2.

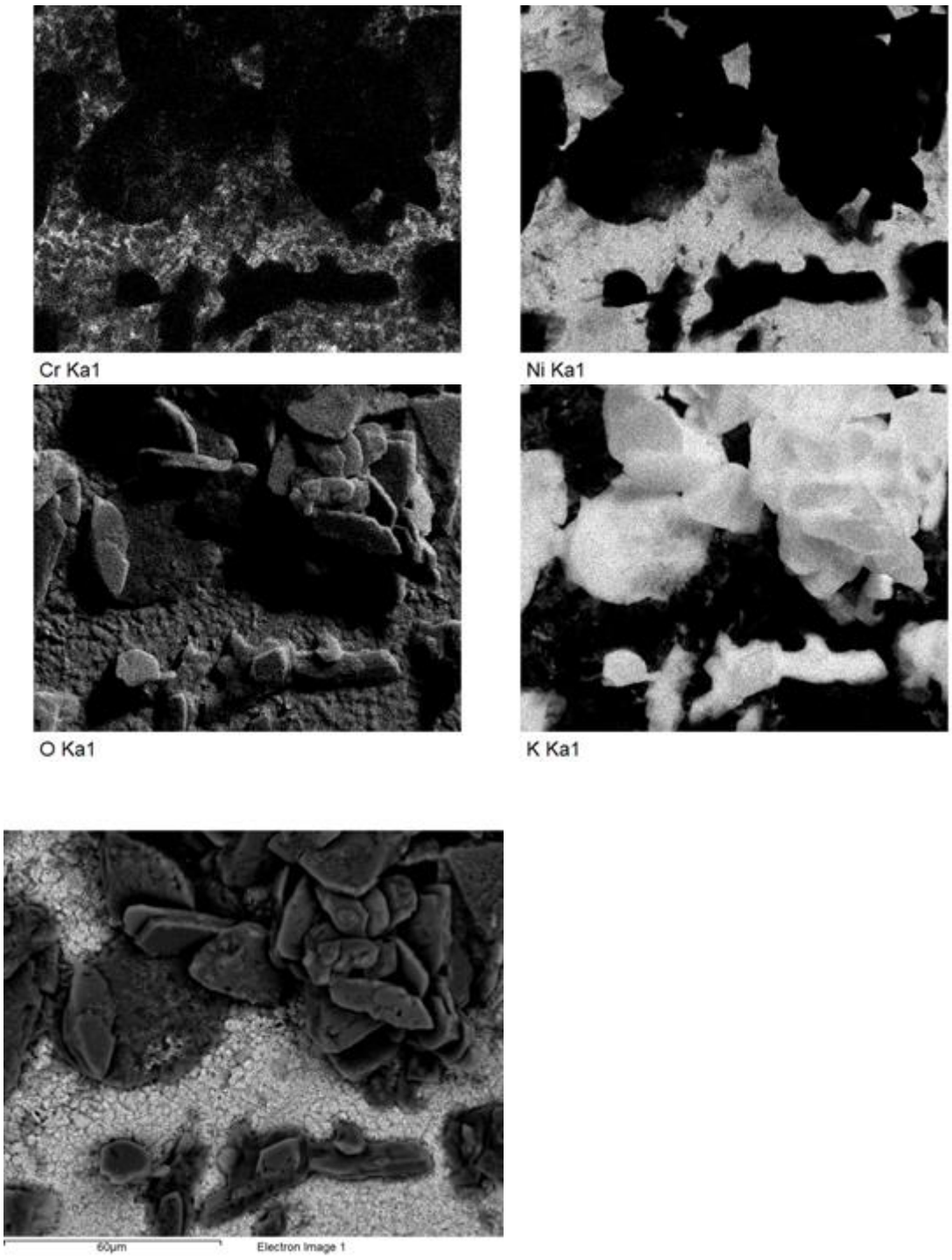

Figure 19. Surface mapping of 82 wt% nickel exposed to K_2CO_3, N_2 and 5% O_2.

KCl exposure with water

After exposure with potassium chloride sprayed on the alloy with 20 wt% nickel, it exhibited the highest mass gain between the samples but also the highest mass gain of all the exposures for alloy 11(see graph 4). The 34 wt% alloy also showed its highest mass gain of all exposing methods but not as great extent as the 20 wt% nickel. The alloy with 82 wt% nickel showed a mass loss as it did when exposed to potassium carbonate.

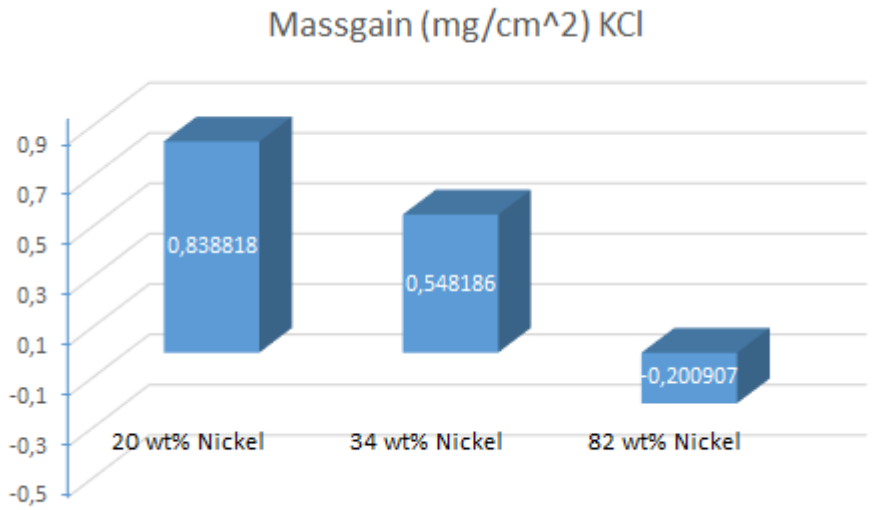

Graph 4. Mass gain after exposure of KCl, H_2O, 5% O_2 and N_2.

Alloy 11 exposure to KCl and water

For the alloy with 20 wt% nickel the KCl exposure showed the highest mass gain for the alloy. Mapping of the surface was done and showed that the oxide growing mainly consisted of iron and oxygen. The oxide grew around blocks of potassium chloride. Which can be seen in figure 20 and figure 21. Mapping also indicated that potassium chromate (K_2CrO_4) formed at various spots.

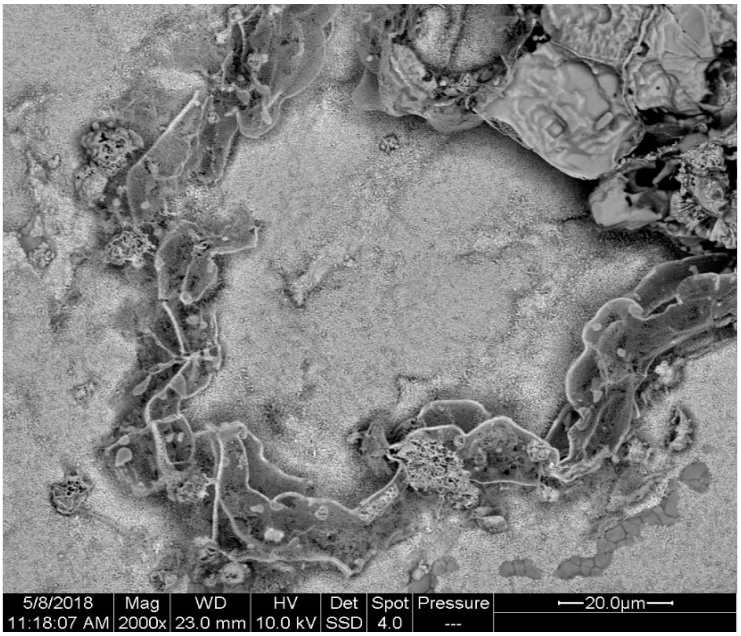

Figure 20. Surface picture of 20 wt% nickel exposed to KCl, H_2O and 5% O_2.

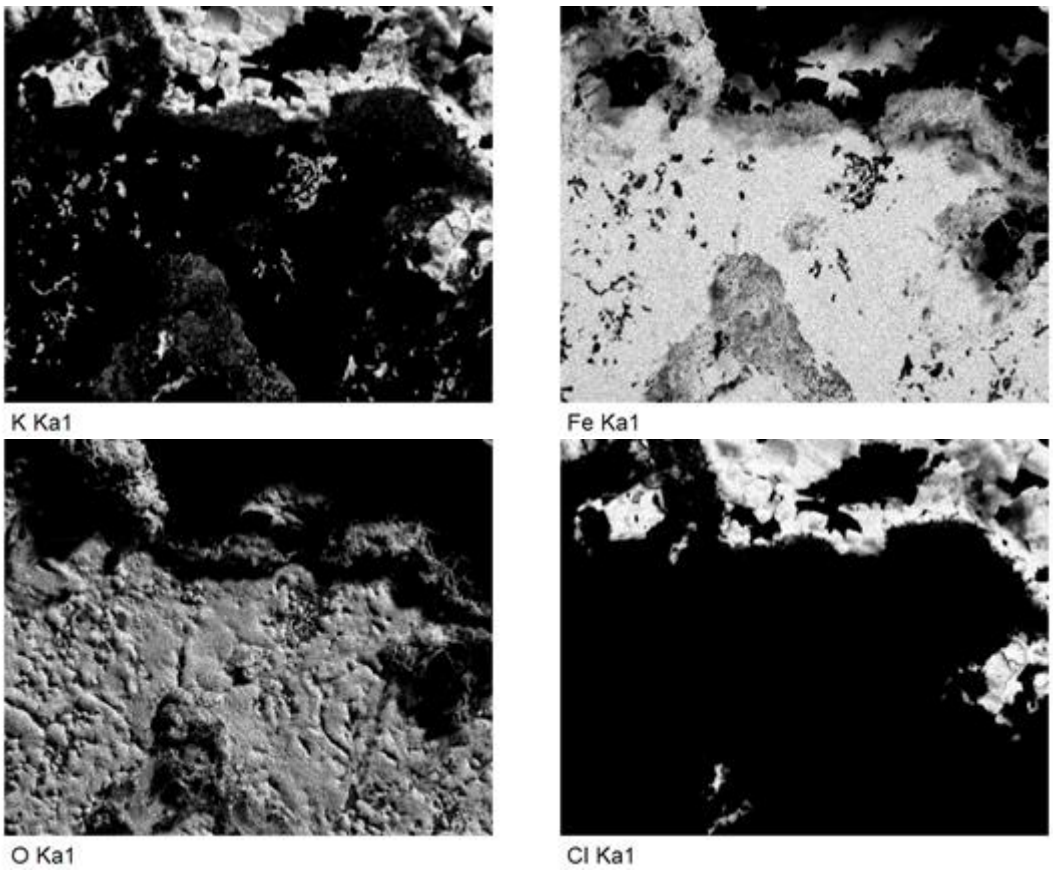

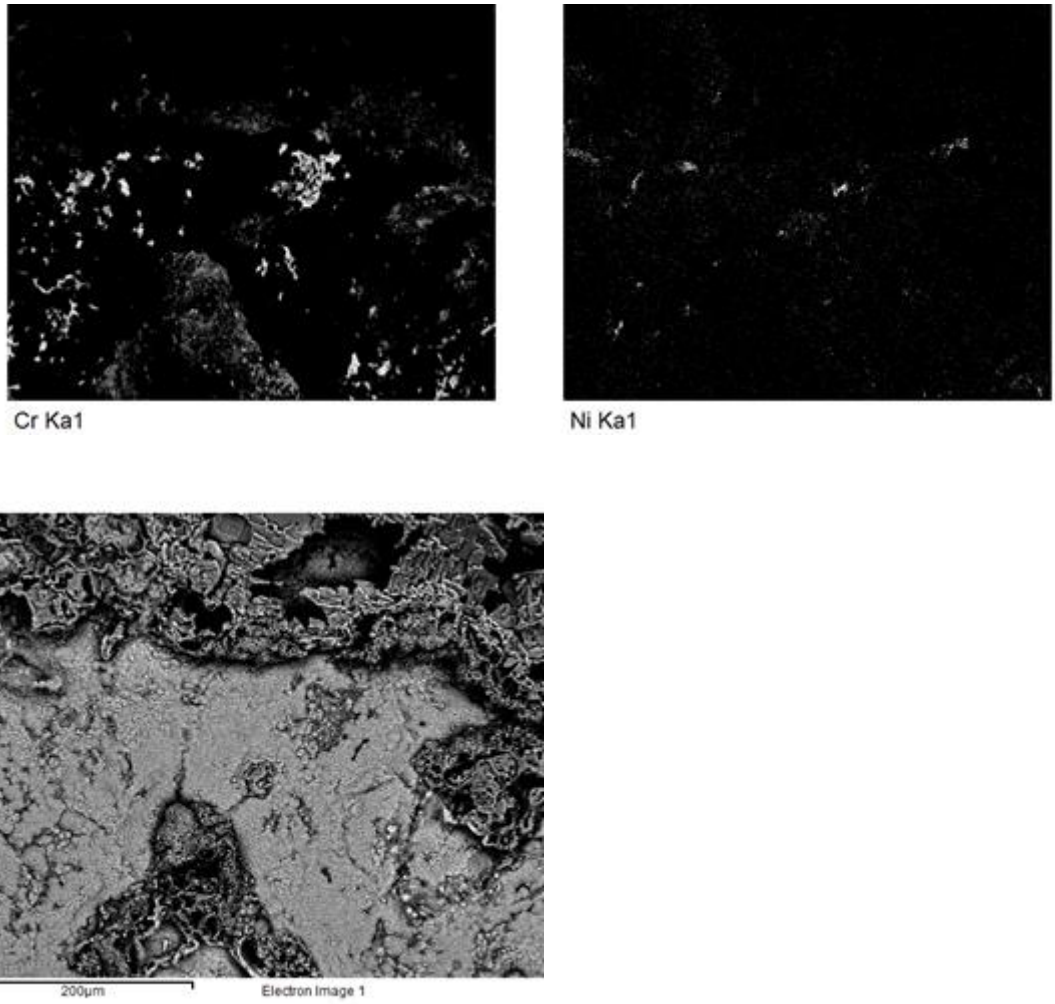

Figure 21. Surface mapping of 20 wt% nickel exposed to KCl, H_2O and 5% O_2.

Alloy 12 exposure to KCl and water

For the alloy with 34 wt% nickel the chloride is only present in small amounts and seem to have evaporated or reacted with water to form HCl. The majority of the oxide that has grown seems to be iron oxide based on the mapping images (figure 23). As the mapping indicates chromium and potassium are present at the same locations together it means K_2CrO_4 has formed where the KCl was sprayed. Nickel enrichments can be observed at several locations suggesting that more nickel oxide has formed there or that the iron oxide is thinner therefore the bulk material shows a stronger signal.

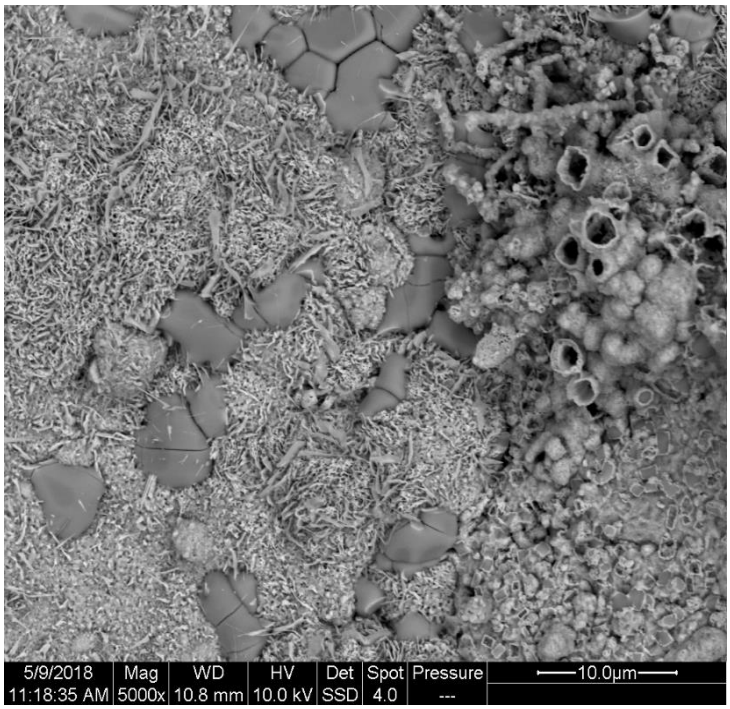

Figure 22. Surface picture of 34 wt% nickel exposed to KCl, H_2O and 5% O_2.

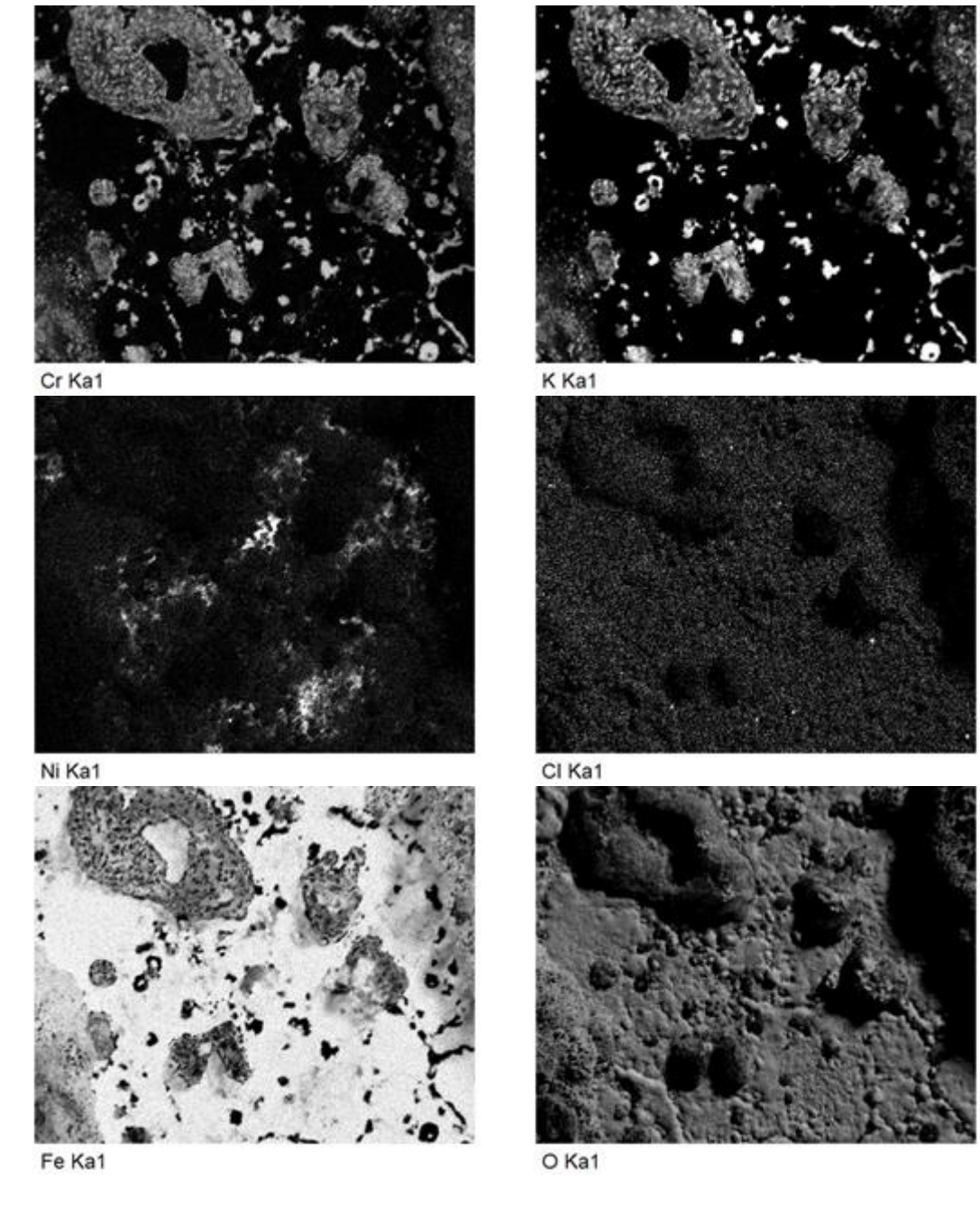

Figure 23. Surface mapping of 34 wt% nickel exposed to KCl, H_2O and 5% O_2.

Alloy 13 exposure to KCl and water

The alloy with 82 wt% nickel which showed a mass loss could be due to the chloride reacting with the water to form HCl or evaporating as KCl (g). The chromium seems to be depleted in most parts but in some locations oxidized and reacted with the potassium at certain potassium rich spots. As can be seen in figure 26, K_2CrO_4 has formed at these locations. Build ups seems to be left from the spraying containing potassium at big parts of the sample. However there seem to be nickel enrichments in big parts of the surface where the chromium is depleted. Comparing the mapping pictures in figure 25 with the point analysis in figure 26, the nickel enriched areas contain high quantities of oxygen suggesting that the nickel would have oxidized to some extent.

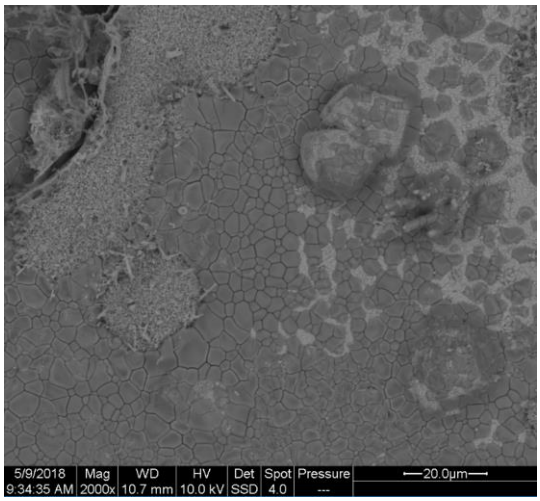

Figure 24. Surface picture of 82 wt% nickel exposed to KCl, H_2O and 5% O_2.

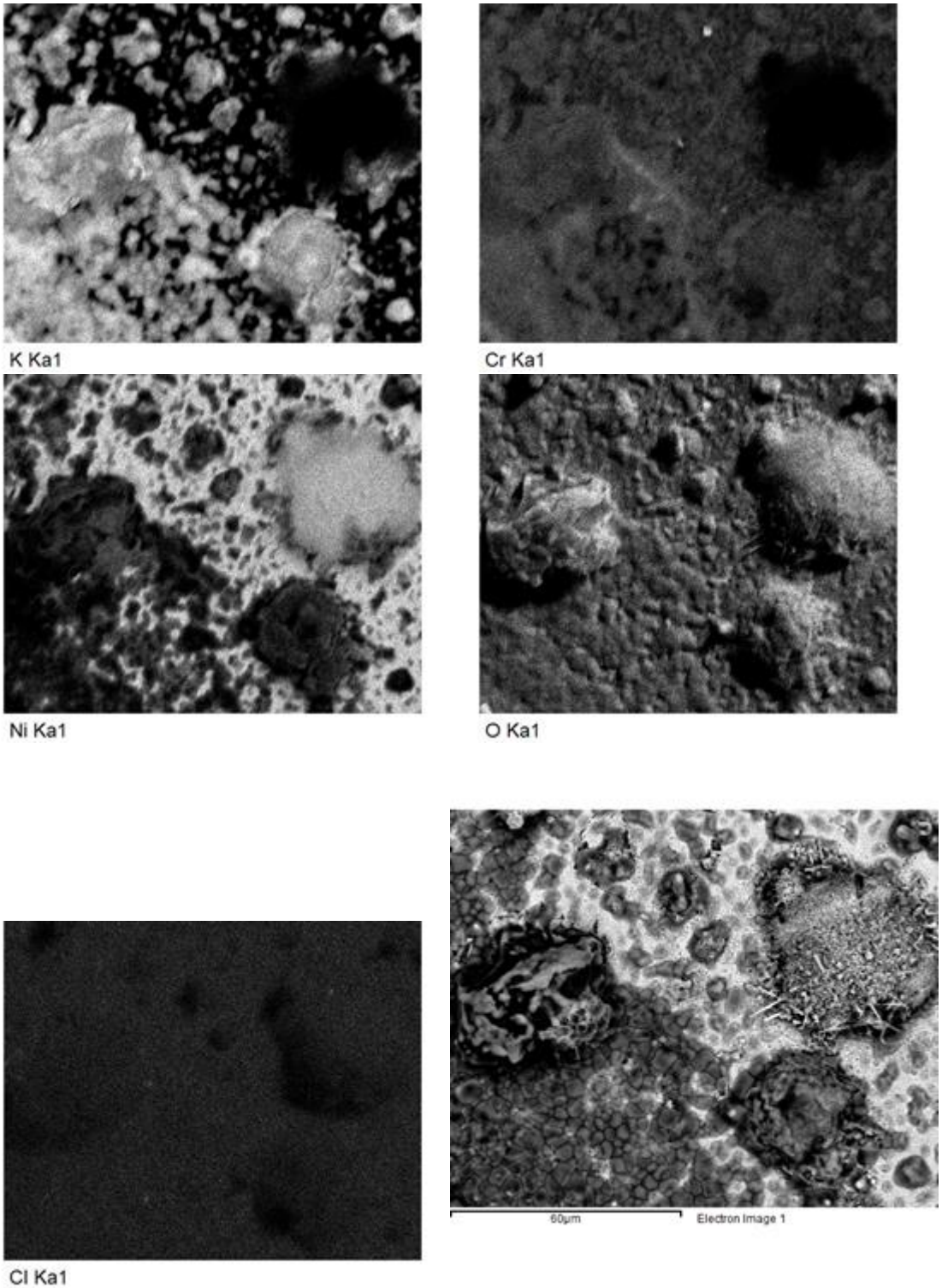

Figure 25. Surface mapping of 82 wt% nickel exposed to KCl, H_2O and 5% O_2.

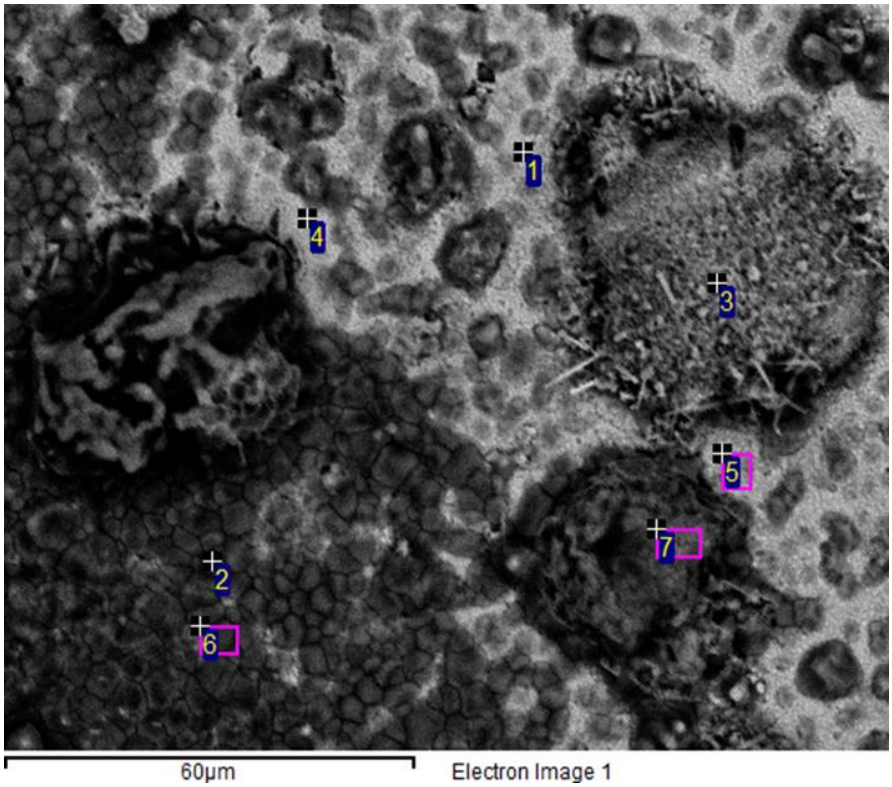

Figure 26. Point analysis of 82 wt% nickel exposed to KCl, H_2O and 5% O_2.

Spectrum	In stats.	O	Cl	K	Cr	Ni
1	Yes	26	0	0	11	63
2	Yes	54	0	25	13	8
3	Yes	45	0	1	2	53
4	Yes	25	0	1	9	64
5	Yes	37	0	3	9	51
6	Yes	47	0	22	14	17
7	Yes	63	0	16	8	13

Table 9. Point analysis of 82 wt% nickel exposed to KCl, H_2O and 5% O_2.

Discussion

Alloy 11, 20 wt% nickel

Alloy 11 with 20 wt% nickel behaved as predicted, showing an increase of oxide growth when exposed to potassium salts. However, the other alloys did not to some extent, show vulnerabilities towards other factors. For alloy 11 the mass gain increased when exposed to potassium salts and even more when exposed to KCl compared to K_2CO_3. This is due to the corrosive properties of the salts which prevents the chromia from remaining protective. Instead a fast growing iron oxide is formed. While exposed to N_2 and 5% O2 the chromia started to form, growing inwards for the alloy with 20 wt% nickel. This aligns with what was predicted as the chromium oxide is growing slowly. Exposure to KCl probably showed the highest mass gain because of the corrosive nature of both potassium and chloride ions at high temperature. The corrosive environment prevents the primary protection from forming and the secondary protection has a very low influence from the nickel forming almost exclusively iron oxide.

Alloy 12, 34 wt% nickel

Alloy 12 with 34 wt% nickel showed its highest mass gain after exposure to KCl as well, probably because the chlorine diffuse through the oxide. The 34 wt% nickel showed to be vulnerable to the presence of water as the highest mass gain was obtained when exposed to water. Why the alloy shows indications of being more prone to high mass gain when exposed to water is unclear. A probable cause is that the microstructure hinders the formation of chromia, perhaps by the grains of the metal being larger, which affects the diffusion of chromium. After the exposure to KCl alloy 11 with 20 wt% nickel had a higher mass gain than alloy 12 with 34 wt% nickel. While exposure to water and air showed alloy 12 to have the higher mass gain. This may indicate that the oxidation for alloy 12 is fast in the beginning but then the formation of oxide regressed and the alloy was more prone to withstand oxidation, and the chlorine attack mechanism. This means that alloy 12 with 34 wt% might have an incubation time for the formation of a compact layer of protective oxide. Meanwhile alloy 11 showed a more linear mass gain. This could be investigated with longer exposures of the alloys.

For alloy 12 the thick oxide layer gained from the water exposure showed clear phases within the oxide which were evaluated using point analysis. The point analysis confirmed the prediction of having iron oxide growing fast outwards, a mix of nickel and iron oxide in the middle and an inwards growing oxide consisting of chromium, nickel and iron oxide. The analysis also showed some expected voids within the oxide and chromium enriched parts where the inwards growing oxide met the bulk material. Clear signs of enrichments at grain boundaries where the oxide was much thinner was observed. As expected the grain boundaries had enrichments of chromium which seemed to protect the boundaries since the chromium oxide grows slower than both nickel and iron oxide. The chromium diffuses faster at the grain boundaries is a possible explanation for the enrichments at the grain boundaries. If alloy 12 were to have an incubation time then this indicates that the iron is accessible at the surface and reacts with oxygen while the nickel and chromium oxides grows at a slower pace but eventually slows down the rapid oxidation of iron.

Alloy 13, 82 wt% nickel

Alloy 13 with 82 wt% nickel was at first predicted to have a higher mass gain than the previous two alloys, based on the mass gain trend and the increase of nickel content. However, although the alloy had a higher content of nickel than the previously two, it had a mass gain slightly higher than the alloy containing 20 wt% nickel. By analyzing the oxide one can observe a continuous layer of oxide across the surface like the alloy containing 34 wt% nickel, although much thinner. The thin continuous layer consists of nickel oxide and since the alloy does not contain iron oxide, which grows faster than nickel oxide, that could be a reason for the lower mass gain.

Putting these results in context with the material used in biomass and waste fired boilers, it will be difficult to say if the different nickel amount showed any signs of desired corrosion resistant behavior. However, judging simply by mass gain won't be enough, and all the alloys had iron/nickel oxide growing after exposures to alkali salts. After 24 hour exposure the primary protection was lost. As the boilers has to be run for long periods of time to be economically viable the second protective mechanism will be vital for the steel inside the boiler. The alloy with 82 wt% nickel seemed to form more chromia and exclusively nickel oxide as it didn't contain any iron. These results are although complicated by the negative mass gains, implying the salt might have evaporated in the furnace, or reacted with water in the case of KCl exposure. This could have resulted in a reduced effect from the salts which is not corresponding well to the environment inside the boiler where the alkali salts are continuously present. However, both alloy 12 containing 34 wt% nickel and alloy 13 with 82 wt% nickel showed signs of slower oxide growth while exposed to alkali salts, compared to alloy 11 with 20 wt% nickel. Longer exposures would be necessary but the mass gains indicate the nickel oxide is growing slower than iron oxide which could mean less oxidation of the metal if the nickel amount is increased. This indicates that the nickel content at higher wt% gives the secondary oxide protection more protective properties towards high temperature corrosion.

Conclusion

Based on the research concluded in this report, the influence of nickel content on the model alloys can be estimated for short time exposures. Longer exposures and with continuous flow of alkali salts would give a more applicable result. What can be concluded is that the formation of nickel oxide (NiO) slows down the corrosion of stainless steels which would improve the lifespan of the metals. Increased amount of nickel indicated more protective properties towards both potassium carbonate and potassium chloride attacks. However, the spray was only applied once and test with continuous flow or regular doses of alkali salts would give more specific result. For the metal inside the boiler other alternatives to change the alloy composition may be viable. Alternatives such as coatings or additives to the fuel that is combusted might have better cost to effect rates. A mixture of all the alternatives may be a good compromise.

References

[1] https://www.footprintnetwork.org/resources/data/. Data and Methodology.

Accessed (2018-03-22).

[2] van der Linden PJ, Hanson CE. Climate change 2007: impacts, adaptation and vulnerability. Parry M, Canziani O, Palutikof J, editors. Cambridge: Cambridge University Press; 2007. (Accessed 2018-03-26).

[3] Cox PM, Betts RA, Jones CD, Spall SA, Totterdell IJ. Acceleration of global warming due to carbon-cycle feedbacks in a coupled climate model. Nature. 2000 Nov;408(6809):184. (Accessed 2018-03-26).

[4] https://ec.europa.eu/energy/en/topics/renewable-energy/biofuels. Biofuels. (Accessed 2018-03-26).

[5] Baxter L. Biomass-coal co-combustion: opportunity for affordable renewable energy. Fuel. 2005 Jul 1;84(10):1295-1302. (Accessed 2018-03-26).

[6] Pettersson J. *Alkali Induced High Temperature Corrosion of Stainless Steel Experiences from Laboratory and Field*. Department of Chemical and Biological Engineering: ; 2008: 22-28, 53-54. (Accessed 2018-03-22).

[7] Brady MP, Wright IG, Gleeson B. Alloy design strategies for promoting protective oxide-scale formation. Jom. 2000 Jan 1;52(1):16-21. (Accessed 2018-04-11).

[8] Nielsen HP, Frandsen FJ, Dam-Johansen K, Baxter LL. The implications of chlorine-associated corrosion on the operation of biomass-fired boilers. Progress in energy and combustion science. 2000 Jun 1;26(3):283-98. (Accessed 2018-03-22).

[9] Van Muylder J. Thermodynamics of corrosion. In Electrochemical Materials Science 1981 (pp. 1-96). Springer, Boston, MA. (Accessed 2018-03-26).

[10] Olivas AM. *High temperature chlorine-induced corrosion of low-alloyed and stainless steels*. Department of Chemistry and Chemical Engineering: ; 2017: (Accessed 2018-03-22).

[11] http://publications.lib.chalmers.se/records/fulltext/171854/171854.pdfAlnegren P. *Oxidation behavior of selected FeCr alloys in environments relevant for solid oxide electrolysis applications*. Department of Chemical and Biological Engineering, CHALMERS UNIVERSITY OF TECHNOLOGY, Gothenburg 2012. (Accessed 2018-05-15).

[12] Uhlig HH. Structure and growth of thin films on metals exposed to oxygen. CORROSION ENGINEERING DIGEST. 1967 Jun 15;16(6):229-37. (Accessed 2018-04-19).

[13] Knoll A, Smigiel E, Broll N, Cornet A. Study of high temperature oxidation kinetics of steel using grazing X-ray reflectometry. In Advances in X-ray Analysis (AXA)-Denver X-ray Conferences 1999 (Vol. 41, p. 170). (Accessed 2018-04-13).

[14] http://www.physics.uwo.ca/~lgonchar/courses/p9826/Lecture12_oxidation.pdf. Dr. Lyudmila Goncharova, The University of Western Ontario, Department of Physics and Astronomy. (Accessed 2018-04-09).

[15] http://www.seas.columbia.edu/earth/wtert/sofos/Albina_Thesis_kinetics_addendum.pdf. Columbia University, New York. (Accessed 2018-04-09).

[16] Pettersson J, Folkeson N, Johansson LG, Svensson JE. The effects of KCl, K 2 SO 4 and K 2 CO 3 on the high temperature corrosion of a 304-type austenitic stainless steel. Oxidation of metals. 2011 Aug 1;76(1-2):93-109. (Accessed 2018-04-13).

[17] Uusitalo MA, Vuoristo PM, Mäntylä TA. High temperature corrosion of coatings and boiler steels below chlorine-containing salt deposits. Corrosion Science. 2004 Jun 1;46(6):1311-31. (Accessed 2018-04-13).

[18] Riedl R, Dahl J, Obernberger I, Narodoslawsky M. Corrosion in fire tube boilers of biomass combustion plants. InProceedings of the China International Corrosion Control Conference 1999 Oct 26 (Vol. 99). (Accessed 2018-04-09).

[19] Ziemniak SE, Hanson M. Corrosion behavior of 304 stainless steel in high temperature, hydrogenated water. Corrosion Science. 2002 Oct 1;44(10):2209-2230. (Accessed 2018-04-06).

[20] Kuang W, Han EH, Wu X, Rao J. Microstructural characteristics of the oxide scale formed on 304 stainless steel in oxygenated high temperature water. Corrosion Science. 2010 Nov 1;52(11):3654-3660. (Accessed 2018-04-06).

[21] Takeda K, Kajimura H, Miyahara M, inventors; Sumitomo Metal Industries Ltd, assignee. Austenitic stainless steel. United States patent US 7,101,446. 2006 Sep 5. (Accessed 2018-05-17).

[22]https://www.neonickel.com/nickel-alloys-for-corrosive-environments/. Nickel Alloys for Corrosive Environments. (Accessed 2018-04-13).

[23] Davis JR, editor. Stainless steels. ASM international; 1994: 4-6, 225-226. (Accessed 2018-04-13).

[24] Kuang W, Wu X, Han EH. The oxidation behaviour of 304 stainless steel in oxygenated high temperature water. Corrosion Science. 2010 Dec 1;52(12):4081-4087. (Accessed 2018-05-22).

[25] Choi SH, Stringer J. The breakaway corrosion of Fe Cr alloys in atmospheres containing sulfur and oxygen. Materials Science and Engineering. 1987 Mar 1;87:237-242. (Accessed 2018-04-11).

[26] Asteman H, Svensson JE, Norell M, Johansson LG. Influence of water vapor and flow rate on the high-temperature oxidation of 304L; effect of chromium oxide hydroxide evaporation. Oxidation of Metals. 2000 Aug 1;54(1-2):11-26. (Accessed 2018-04-13).

[27] Akgün OV, Ürgen M, Çakir AF. The effect of heat treatment on corrosion behavior of laser surface melted 304L stainless steel. Materials Science and Engineering: A. 1995 Nov 15;203(1-2):324-331. (Accessed 2018-04-18).

[28] Hanyi L, Fuhui W, Bangjie X, Lixin Z. High-temperature oxidation resistance of sputtered micro-grain superalloy K38G. Oxidation of metals. 1992 Oct 1;38(3-4):299-307. (Accessed 2018-04-18).

[29] Aghuy AA, Zakeri M, Moayed MH, Mazinani M. Effect of grain size on pitting corrosion of 304L austenitic stainless steel. Corrosion Science. 2015 May 1;94:368-376. (Accessed 2018-04-24).

[30] Graham MJ, Hussey RJ. Analytical techniques in high temperature corrosion. Oxidation of metals. 1995 Aug 1;44(1-2):339-374. (Accessed 2018-04-06).

[31] Swapp S. Scanning Electron Microscopy (SEM): University of Wyoming. (Accessed 2018-04-18).

[32] https://www.chalmers.se/en/researchinfrastructure/CMAL/instruments/SEM/Pages/default.aspx Scanning Electron Microscopy (SEM). (Accessed 2018-04-25).

[33] https://www.topanalytica.com/BIB. Broad Ion Beam cutting (BIB). (Accessed 2018-04-25).

[34] https://www.chalmers.se/en/researchinfrastructure/CMAL/instruments/FIB/BIB/Pages/default.aspx. Broad Ion-Beam. (Accessed 2018-04-19).